Technical report; TR-273

KNMI

Estimation of future discharges of the River Rhine in the SWURVE project

T.A. Buishand and G. Lenderink

De Bilt, 2004

Technical report = technisch rapport; TR-273

De Bilt, 2004

PO Box 201
3730 AE De Bilt
Wilhelminalaan 10
De Bilt
The Netherlands
http://www.knmi.nl
Telephone +31(0)30-220 69 11
Telefax +31(0)30-221 04 07

Authors: T.A. Buishand
G. Lenderink

ISSN: 0169-1708

ISBN: 90-369-2264-X

Estimation of future discharges of the river Rhine in the SWURVE project

T.A. Buishand and G. Lenderink

with contributions from
M.V. Shabalova and W.P.A. van Deursen

Technical Report TR-273

Table of contents

Summary

The change in the flow regime of the river Rhine by the end of the 21st century was one of the eight case studies in the European project SWURVE (Sustainable Water: Uncertainty, Risk and Vulnerability in Europe). Both the potential changes in high river flows (flood protection) and low river flows (inland navigation) were of interest. The river flow simulations were done with the RhineFlow model, a distributed water balance model of the Rhine basin with a temporal resolution of 10 days and a spatial resolution of 3 km × 3 km. For SWURVE the model was recalibrated with a larger meteorological dataset than used in earlier studies of climate change impacts on the discharge of the river Rhine.

The output of the Hadley Centre regional climate models HadRM2 and HadRM3H was extensively used in the SWURVE project. These regional models cover nearly the whole of Europe and part of the Atlantic Ocean with a grid resolution of 50 km × 50 km, and are driven at their boundaries by a global model. For the older HadRM2 model two simulation runs were available: a 30-year control run, representing the climate of the second half of the 20th century, and a 20-year anomaly run, representing the climate for the period 2080 – 2099. A 1% increase in equivalent CO_2 after 1989 was assumed. Sulphate aerosol forcing was not included. The HadRM3H simulations were performed with SRES emission scenarios. For the A2 emission scenario three simulation runs were available for the period 2070-2099. There were also three simulation runs for the period 1961-1990 (control climate).

The precipitation and temperature biases in the control simulation are of similar magnitude for the HadRM2 and HadRM3H simulations (about 1 °C for the seasonal mean temperature and up to 40% for the seasonal mean precipitation over the basin). Both models show an increase of 4.5 °C in the basin-averaged annual mean temperature at the end of the 21st century. The mean precipitation increases in winter and decreases in summer. The decrease in summer precipitation in the HadRM3H simulations is as large as 40%. In both the HadRM2 and HadRM3H simulations, the decrease in mean summer precipitation is accompanied by a significant increase in the coefficient of variation (*CV*: standard deviation divided by the mean) of the 10-day precipitation totals. The HadRM2 simulations also show a significant increase in the *CV* in the winter season, but the *CV* decreases in winter in the HadRM3H simulations. The latter is accompanied by a relatively small increase in the largest quantiles of the 10-day precipitation distribution in winter.

Different scenario time series for application in the RhineFlow model were produced from the regional climate model output. The observed data were perturbed in two different ways with the seasonal mean changes in the HadRM2 experiment. For the HadRM3H simulations a simple perturbation of the data for present-day conditions was compared with the direct use of the climate model output in RhineFlow. The HadRM2 scenario 1 was obtained by perturbing the observed precipitation and temperature data with the seasonal mean changes in the HadRM2 experiment. The change in potential evaporation was based on an empirical relation between the changes in open water evaporation and temperature. The *CV* of the 10-day precipitation totals remains unchanged in this simple scenario. A more advanced scenario was produced by adjusting the standard deviations of the observed precipitation and temperature data as well (HadRM2 scenario 2). Unlike the HadRM2 scenario 1, the seasonal changes in the mean precipitation and temperature in the HadRM3H simulations were applied to the bias-corrected control runs rather than to the observed data (HadRM3H scenario 1). The bias-corrected model output was also directly used as input into the RhineFlow model (HadRM3H

scenario 2). The estimated potential evaporation from the HadRM3H output could not be used in these scenarios. The dependence between this potential evaporation and the simulated soil moisture by RhineFlow appeared to be too strong, resulting in a bias in the simulated summer flows. This bias could be suppressed by deriving potential evaporation from temperature only.

All four scenarios result in an increase in the mean winter discharge at Lobith (German – Netherlands border) of 20-30%. The mean summer discharge decreases by 30% in the HadRM2 scenarios and by 40% in the HadRM3H scenarios. The realism of the latter could be questioned because of indications of a too strong hydrological feedback in the HadRM3H control climate, i.e. dry conditions (and also wet conditions) tend to be too persistent. The changes in the seasonal mean flows are accompanied by more extreme flood peaks and an increased frequency of low flows.

In contrast to the change in the seasonal mean flows, the changes in the annual maximum flows are very sensitive to the method of scenario construction. The relative increase of the 1000-year event is for the HadRM2 scenario 2 more than twice as large as that for the HadRM2 scenario 1, mainly because the latter did not account for the increase in the *CV* of the 10-day precipitation totals in winter. The direct use of the HadRM3H output (HadRM3H scenario 2) resulted in a much smaller increase in the 1000-year event than the perturbation of the control run (HadRM3H scenario 1). The HadRM3H scenario 2 should be considered as the more appropriate one because it includes the changes in the variability and the shape of the distributions of the meteorological inputs as well as the changes in their correlations. The relative increase of about 10% of the 1000-year event in the HadRM3H scenario 2 is small compared to the relative increase of 37% in the most appropriate scenario (HadRM2 scenario 2) from the HadRM2 simulations. An important factor causing these differences is that the *CV* of the 10-day precipitation totals in winter increases in the HadRM2 simulations and decreases in the HadRM3H simulations. Apart from the large climate-model dependence of the change in the 1000-year event, there are additional uncertainties due to the limited length of the scenario series (35 years for the HadRM2 scenarios and 90 years for the HadRM3H scenarios) and the extrapolation beyond present-day conditions.

The change in the frequency of low flows is much less sensitive to the method of scenario construction than the change in the annual maximum distribution. The results depend, however, on the regional climate model used. The proportion of the 10-day periods that the Rhine discharge is below 1000 m^3/s (about 5% for present-day conditions) roughly doubles in the HadRM2 scenarios and quadruples in the HadRM3H scenarios. For the latter scenarios the additional transport costs due to drought increase from about 80 million euro a year for present-day conditions to about 500 million euro a year, assuming no changes in the number of vessels and in the vessel types. This cost estimate should be used with care because of the low confidence in the summer drying as simulated by the HadRM3H model and because of systematic errors in the RhineFlow simulations of low flows.

1. Introduction

The Rhine is one of the major hydrological systems in Europe, affecting the economy and environment of one of the most densely populated areas of Europe. The river rises in the Swiss Alps and flows via Germany and the Netherlands to the North Sea (Figure 1). The Rhine is 1320 km long and its basin covers an area of 185,000 km^2. Dikes protect the lower parts of the basin from flooding. The Rhine is the busiest waterway for the transport of goods in Western Europe. In addition, its water is used for drinking water, sprinkling crops, cooling water, hydropower industry and prevention of salt-water intrusion from the North Sea into polder areas. Climate-related changes in water levels and water availability will affect flood protection and all river-related activities.

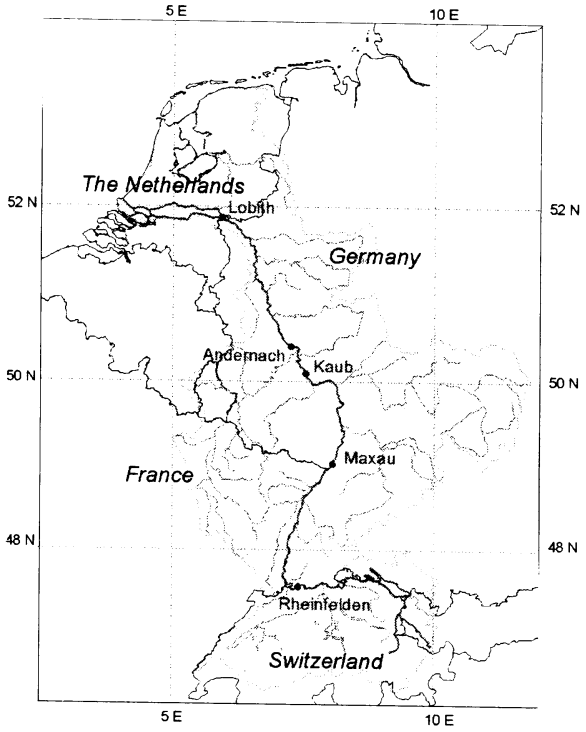

Figure 1. Basin of the river Rhine, with the locations of five gauging stations

It is therefore not surprising that, especially in the Netherlands, a number of projects were devoted to assessments of climate change impacts on the hydrology of the Rhine (Kwadijk, 1993; Grabs, 1997; Middelkoop, 2000). A conceptual water balance model for the Rhine basin was specifically designed to accomplish these ends (Kwadijk, 1993; van Deursen and Kwadijk, 1993). A tendency for an increase in winter runoff and a decrease in summer runoff of the Rhine in simulated future climates has been revealed. However, climate change scenarios used in those studies were based on rather old runs of general circulation models (from the late 1980s to early 1990s) and did not account for a possible change in the variability of climatic inputs. Future temperature scenarios were simply obtained by adding the expected seasonal mean temperature change to the observed temperature series, and by multiplying the observed precipitation series with the expected relative change in the seasonal mean precipitation.

In the last few years, the quality of climate simulations with high-resolution climate models has improved significantly (e.g. Frei et al., 2003, Räisänen et al., 2004). The typical resolution of regional climate models is at present about 50 km, compared to about 300 km for their driving general circulation model. Apart from the increase in computer power, the improved representation of physical processes (such as radiation, boundary-layer processes, soil processes, and cloud microphysics) has led to a better simulation of the present-day climate (Vidale et al., 2003). In the SWURVE project two regional climate model simulations from the Hadley Centre of the UK Meteorological Office and an updated version of the hydrological model of the Rhine were used to assess the potential changes in the river flows. From the older regional climate model simulation, HadRM2, two climate change scenarios were derived: one scenario by perturbing the observed data with the seasonal mean changes, similar to earlier studies, and one scenario by perturbing the observed data in a more complex way to include the simulated changes in variability. For the more recent HadRM3H simulation the classical method of perturbing the data for the present–day climate was compared with the direct use of the climate model output as input into the hydrological model. All climate change scenarios refer to the climate at the end of the 21st century.

Section 2 describes the hydrological model. The temperature, precipitation and evaporation simulations of the HadRM2 and HadRM3H models are discussed in section 3, both for the present-day and future climate. Section 4 deals with the bias corrections of the HadRM3H simulations that are needed to reproduce the mean annual cycle of the discharge of the river Rhine. The application of the various climate change scenarios is presented in section 5. Besides the changes in the monthly mean flows, much attention is given to the change in the design discharge for flood protection in the Netherlands and to changes in low flow conditions on inland navigation. Section 6 summarizes the main results and gives some recommendations for further research.

2. RhineFlow model

2.1. Model description

The RhineFlow hydrological model is a spatially distributed water balance model of the Rhine basin that can simulate river flow, soil moisture, snow pack and groundwater storage with a monthly (first version) or 10-day time step. With this relatively long time step hydraulic routing can be ignored. A full description of the RhineFlow model is given in Kwadijk (1993), van Deursen and Kwadijk (1993), and Kwadijk and Rotmans (1995), so only a brief summary of the model is given here, with some detail on the recent model update.

RhineFlow uses a spatial database implemented in a raster Geographical Information System. The spatial resolution is 3 km x 3 km in the present study. The model calculates the amount of water in the water balance compartments of the basin from meteorological data. Apart from geographical data on topography, land use, soil type and groundwater flow characteristics, the following meteorological input variables are used: the 10-day averages of the maximum, minimum and mean temperature, and the 10-day totals of potential evaporation and precipitation. The minimum and maximum temperatures are used in the calculation of snow

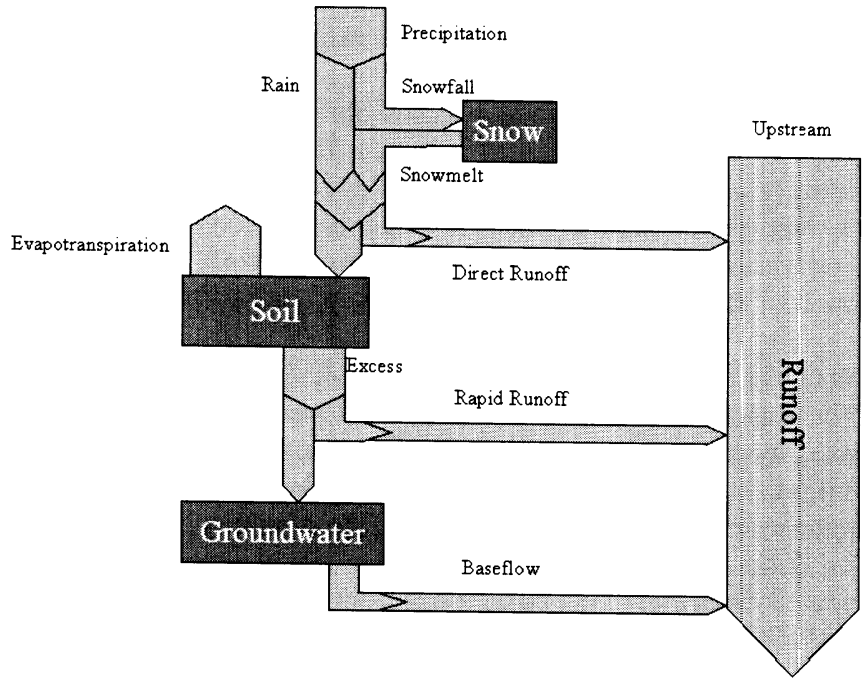

Figure 2. Schematic of the RhineFlow model.

accumulation and snow melt. Potential evaporation is represented as the product of a crop factor[1] and reference evaporation E_r, which was provided by different Met Services. The equations and input data used for calculating E_r are not exactly known. For the Swiss part of the basin, however, potential evaporation has been derived from temperature using the Thornthwaite formula as indicated in Kwadijk and Rotmans (1995). The conversion of potential to actual evaporation is based on Thornthwaite and Mather (1957).

The model consists of several routines (Figure 2), describing water flows between the storages. The three main storages are the soil moisture storage, the groundwater storage and the snow (glacial) storage. The soil moisture content is formed from precipitation plus snowmelt minus actual evaporation minus direct runoff and depends on soil and land use types. If the soil moisture capacity is exceeded, then the surplus is separated into the rapid runoff and the groundwater reservoir; the latter adds a portion of water (the delayed runoff) to the total runoff. For each cell at each time step, the model output consists of the accumulated runoff from all the upstream cells, calculated according to the drainage pattern. For certain cells this output represents the discharge series at gauging stations along the river Rhine.

2.2. Model update

The meteorological dataset of the RhineFlow model has been updated with new daily data from the database of the International Commission for the Hydrology of the Rhine basin (CHR). The spatial coverage has been substantially improved. The temperature is now available for more than 70 stations in the Rhine basin. The precipitation series are available

[1] The crop factors for the first version of RhineFlow are given in Kwadijk (1993). In later versions the crop factor for forest has been changed from 1.1 to 1.5.

for about 200 subcatchments in Germany, over 30 stations in France and for a 2 km x 2 km spatial grid in Switzerland. The 35-year period 1961-1995 was selected as the baseline.

With this meteorological update, the RhineFlow model was recalibrated using the observed discharge data at five gauging stations along the Rhine (Figure 1). The set of calibration parameters includes an adjustment parameter for the potential evaporation, which is used to close the total water balance (that is to assure that the measured precipitation minus simulated actual evaporation equals the measured discharge over the calibration period), and parameters for the separation and recession of the water flows to and from the groundwater reservoir.

The first recalibration was done for the application with the HadRM2 data. Although a reasonable reproduction of the seasonal mean flows and the annual maximum flows was achieved, the RhineFlow model systematically underestimated the annual minimum flows (Shabalova et al., 2003). To improve the reproduction of low flows, the model was recalibrated again for the application with the HadRM3H data. This version of the model is denoted as RhineFlow-3 (van Deursen, 2003). The values of the model parameters were estimated by fitting the computed discharge to the observed discharge for each of the five gauging stations for the period 1961-1974. For Lobith at the German-Netherlands border this resulted in a Nash-Sutcliffe (1970) efficiency of 0.60. The left panel of Figure 3 shows the time evolution of the annual mean flows. The correspondence between the modelled and observed flows is quite good for the calibration period. From the early 1970s, however, the model systematically overestimates the observed annual flows. The reason for this overestimation is not known.

The reproduction of the 10-day annual maximum flows at Lobith is presented in the right panel of Figure 3. The annual maximum refers here to the largest value in the water year running from September of the previous year till September. Except for a slight tendency to underestimate the largest 10-day values, the RhineFlow-3 model reproduces the annual maximum flows well.

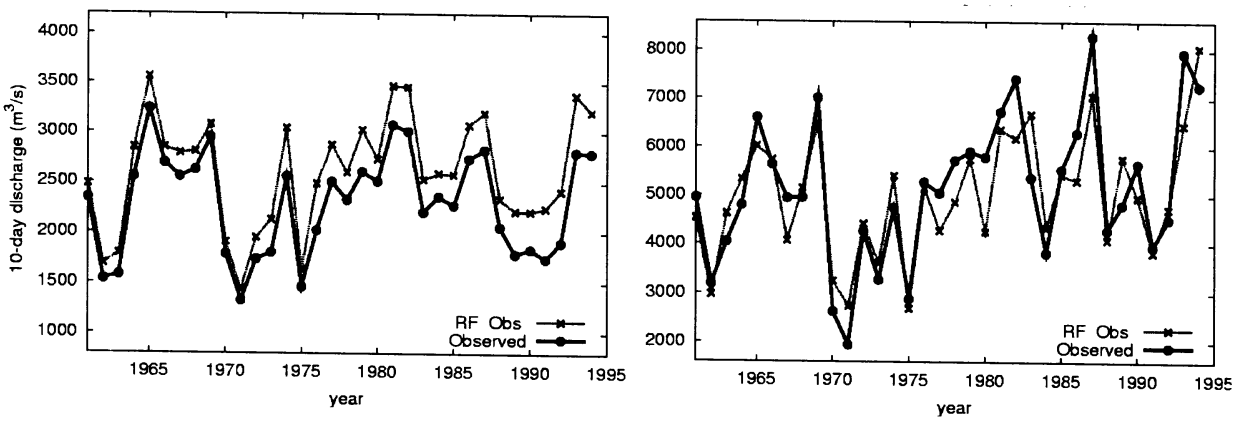

Figure 3. Observed annual mean discharge (left panel) and annual maximum discharge (right panel) at Lobith compared with those simulated by Rhineflow. The observed values were derived from the DONAR database.

3. Regional climate model simulations[2]

3.1. The HadRM2 and HadRM3H experiments

a. HadRM2

The HadRM2 model is a limited area model that covers nearly the whole of Europe and a part of the Atlantic Ocean with a grid resolution of about 50 km x 50 km. The model is driven at its boundaries by output from the global coupled climate model HadCM2 (Johns et al., 1997). The finer resolution of HadRM2 provides for a more realistic simulation of precipitation than that of HadCM2 (Noguer et al., 1998; Durman et al., 2001). The output from two integrations of HadCM2/HadRM2 was used. The control climate simulation was conducted with a constant greenhouse gas forcing representative of the second half of the 20th century. Thirty years of simulation were available for analysis. The boundary conditions for the future climate in HadRM2 were taken from a transient climate change experiment with HadCM2 using historical greenhouse gas forcing from 1860 to 1989 and a 1% per year increase in equivalent CO_2 after this. No sulphate aerosol forcing was included. This leads to an increase in the global mean temperature of 3.0 ^{0}C in the 2080s. Twenty years (2080-2099) of perturbed climate simulation with HadRM2 were available. The climate change estimates in this report were derived from the 20-year perturbed run and the last 20 years of the control run. The complete control run was used, however, in comparisons with the observed climate.

There are 89 HadRM2 grid boxes in the Rhine basin. The fields of mean, maximum and minimum temperature, and precipitation were extracted for the Rhine area with daily resolution and averaged or accumulated over 10 days. Changes in potential evaporation were derived from the changes in the mean temperature using a relation between the change in open water evaporation and temperature for the Netherlands due to Brandsma (1995). Possible effects of changes in incoming solar radiation, relative humidity and wind speed on evaporation are neglected in this approach. Despite this shortcoming, it turns out that the changes in the actual evaporation for the summer half-year from the RhineFlow model correspond quite well with those simulated by HadRM2 (section 5.2).

b. HadRM3H

The HadRM3H model covers about the same area as the HadRM2 model, also with a resolution of about 50 km × 50 km. The lateral boundaries are given by output from a high-resolution (≈ 120 km × 120 km) global atmospheric model HadAM3H. The HadAM3H model was run for the period 1961 - 1990 (control climate) with observed sea-surface temperature and sea-ice for that period. A second run was performed for the future period 2070 – 2099 with the simulated changes in sea-surface temperature and sea-ice of the global coupled climate model HadCM3 (Johns et al., 2003) added to the observations. This approach resulted in a more realistic simulation of the North Atlantic storm track than would have been the case if HadRM3H were directly nested in the global coupled climate model (UKCIP, 2002). Two different SRES[3] scenarios of greenhouse gases and sulphate aerosol emission were considered. In the first scenario A2, the total carbon emission to the atmosphere gradually increases throughout the century, and the global temperature is projected to increase by 3.3°C in the 2080s. This increase is comparable with that in the HadRM2 experiment. The

[2] A more detailed treatment of the application with the HadRM2 data is given in Shabalova et al. (2003). Parts of the application with the HadRM3H data have been submitted to Hydrol Earth Syst Sci (Ekström et al., 2004; Lenderink et al., 2004).

[3] The Special Report on Emissions Scenarios by IPCC (Nakićenović and Swart, 2000).

second scenario B2 assumes a slow increase of carbon emission up to about 2050 and an emission reduction afterwards; the global temperature increases by 2.3°C in the 2080s. There are three-member ensemble simulations for the control climate and for scenario A2 and there is one simulation for scenario B2.

There are 97 HadRM3H grid boxes in the Rhine basin. Mean, maximum and minimum temperature, and precipitation are direct model output, averaged or accumulated over 10 days. Potential evaporation E_p for a clipped grass-surface was provided by the Climatic Research Unit. E_p was calculated from the daily values of temperature, the fraction of total cloud as estimated from longwave radiation (as a substitute for the relative sunshine duration), relative humidity and wind speed in the HadRM3H output using the FAO Penman - Monteith method (Allen et al., 1994). The choice of this method was based on an inter-comparison of different formulations for estimating potential evaporation in the framework of the EU funded project WRINCLE.

3.2. Control climate

To estimate the bias in the control climate simulation of HadRM2/3H, the simulated temperature and precipitation fields were compared with 35 years (1961-1995) of observations in the area.

a. Temperature

Table 1 shows the mean seasonal temperatures as observed and simulated in the control climate experiments of the regional models. The simulated HadRM3H values are expressed in terms of the mean of the three-member ensemble run. The scatter of the values among the individual members of the ensemble is small, within 0.3°C for each season except winter (0.7°C). The bias in the annual mean temperature of the HadRM2/3H simulations is within 1°C for the entire basin. Seasonally, the bias in HadRM2 is largest (≈1.5°C) in spring and summer, whereas HadRM3H has its largest bias (≈1°C) in winter and summer. Other regional climate models give similar biases. According to the IPCC Third Assessment Report (Giorgi et al., 1991) the area–average bias is generally within 2°C for regions of 10^5 to 10^6 km^2. At sub-basin spatial scales, the seasonal bias of the HadRM2/3H simulations is still within 1.5°C for most seasons.

Table 1. Seasonal temperature in °C as observed (mean 1961-1995) and simulated in the HadRM2/3H control climate experiments. Shown are averages over the entire Rhine basin.

	DJF	MAM	JJA	SON	Year
Observations	0.18	7.38	15.92	8.40	7.97
HadRM2	0.72	5.72	14.68	8.09	7.13
HadRM3H	1.12	7.18	17.05	8.87	8.56

b. Precipitation

Table 2 shows the mean seasonal precipitation as observed and simulated in the control climate experiments of the regional models. There is a considerable scatter of the seasonal mean values among the HadRM3H ensemble members, with the largest difference of 12% in

Table 2. Same as in Table 1, but for mean precipitation in mm/day. The HadRM3H values refer to one member of the ensemble.

	DJF	MAM	JJA	SON	Year
Observations	2.60	2.61	3.21	2.59	2.73
HadRM2	3.73	3.38	3.59	2.88	3.13
HadRM3H	3.63	3.40	3.26	3.22	3.38

the Alpine region in winter. The scatter is due to the large year-to-year variation of the precipitation totals and not to systematic differences between the ensemble members. HadRM2 and HadRM3H overestimate the basin-averaged annual mean precipitation by 15% and 20%, respectively. The largest wet bias is found in the Alps, where the annual mean precipitation is overestimated by about 30%. In the middle and lower parts of the Rhine basin the annual mean bias is about 15%. Seasonally, the bias is largest in winter, especially in the Alps, and smallest in summer. A considerable wet bias in winter and spring in the European domain was also found in simulations with the Rossby Centre regional climate model both with boundaries from HadCM2 and the ECHAM4 global coupled climate model (Rummukainen et al., 2001). This bias is partly due to the fact that the observed precipitation amounts were not corrected for the systematic undercatch inherent to rain gauges.

For the HadRM3H ensemble, Figure 4 shows the bias in winter and summer precipitation at the grid box scale. In winter there is a large positive bias (more than 100% of observed precipitation) at the highest grid boxes in Switzerland and a negative bias (50% of observed precipitation) at the adjacent lower grid boxes. A similar pattern of the precipitation bias is found in spring and autumn. Grid-box variations are less pronounced in summer.

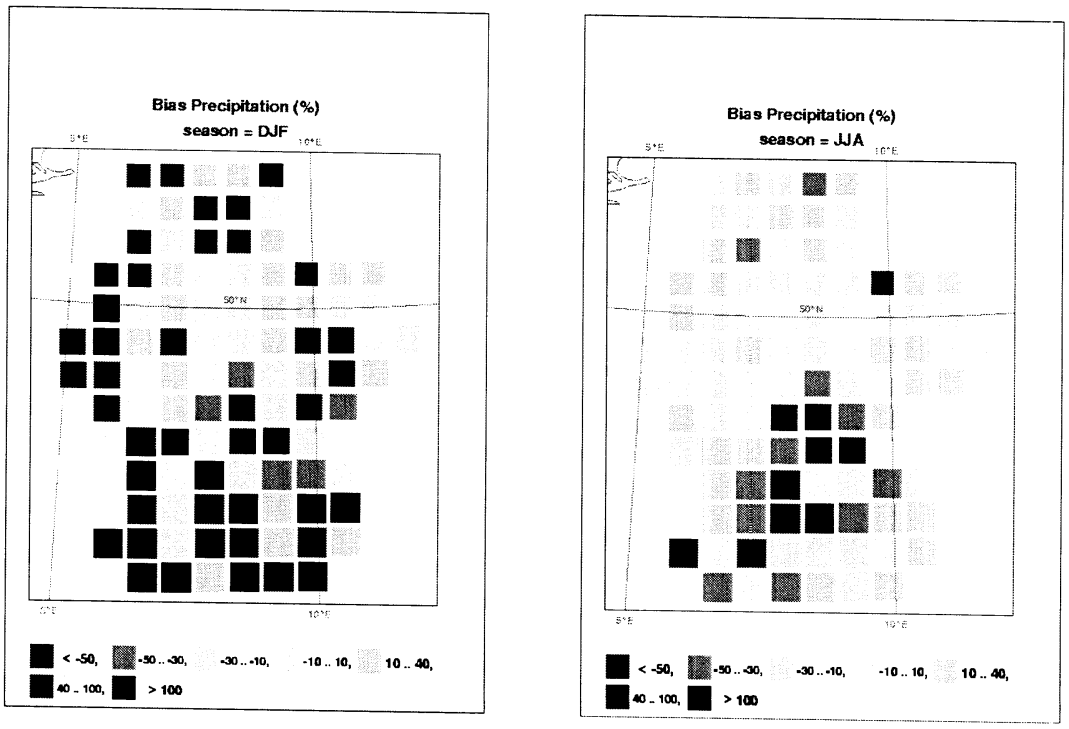

Figure 4. Bias(%) of the mean winter (DJF) and summer (JJA) precipitation in the HadRM3H simulations (relative to the observed means).

c. Precipitation variability

The coefficient of variation (*CV*: standard deviation divided by the mean) was considered as a measure of variability of the 10-day precipitation totals. *CV* does not change if the precipitation totals are multiplied by a constant factor. From Table 3 it can be seen that *CV* is well reproduced by the model simulations. HadRM2 somewhat underestimates the observed *CV* and HadRM3H has a slight tendency to overestimate *CV* (on average by about 10%). The coefficient of skewness (a third-order statistic) is also somewhat overestimated by this regional climate model (on average by about 17%).

Table 3. Coefficient of variation (*CV*) of the 10-day precipitation totals for the observed precipitation (period 1961-1995) and for the simulated precipitation in the control runs of HadRM2/3H. The HadRM3H values refer to one member of the ensemble run.

	DJF	MAM	JJA	SON	Year
Observations	0.90	0.73	0.70	0.90	0.81
HadRM2	0.71	0.65	0.71	0.93	0.75
HadRM3H	0.95	0.79	0.82	0.99	0.89

d. Spatial correlations

In spite of the large local biases, the HadRM3H model reproduces the geographical structure of the observed temperature and precipitation fields reasonably. The pattern correlation with observations is 0.71 for mean annual precipitation and 0.95 for mean annual temperature, with only small seasonal variations. The HadRM2 control simulation has the same pattern correlation for mean annual temperature, but for mean annual precipitation the pattern correlation with the observed annual mean field is only 0.54. The pattern correlation of the annual temperature and precipitation fields is –0.86/–0.74 in HadRM2/3H versus –0.75 in the observations.

e. Potential evaporation

The potential evaporation E_p from the HadRM3H output can be compared with the values derived from observed meteorological data (Figure 5). The latter attain their maximum in early July and those from the HadRM3H output in mid August. The relatively early peak for

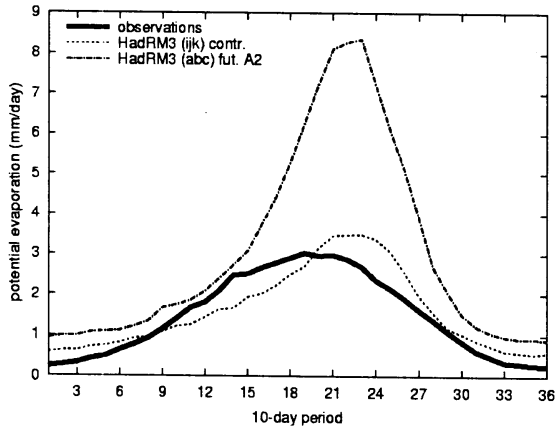

Figure 5. Mean potential evaporation for the 36 periods of 10 days in the year from observations (solid line), the HadRM3H control simulations (dotted lines), and the HadRM3H-A2 future simulations (dash-dotted line).

the "observed" data points at a relatively large effect of the incoming solar radiation. Apart from this shift of the summer peak, the HadRM3H values tend to be larger during winter.

3.3. Future climate

a. Mean temperature

Table 4 shows the simulated temperature changes under three forcing scenarios. Shown are averages over seasons and over the entire basin as in Table 1. The scatter of the values among the individual ensemble members of the A2 simulation is small, of the same order of magnitude as in the case of the control climate simulations.

Table 4. Seasonal temperature changes in °C, as simulated by HadRM2 (mean for 2080-2099 minus mean for the control run) and by HadRM3H (mean for 2070-2099 minus mean for 1961-1990) under two forcing scenarios, A2 (mean of the three-member ensemble) and B2.

	DJF	MAM	JJA	SON	Year
HadRM2	5.76	3.97	4.74	4.72	4.77
HadRM3H-A2	3.97	3.53	6.16	4.94	4.65
HadRM3H-B2	2.38	2.14	4.36	3.22	3.02

On average, the HadRM3H-A2 experiment results in the same temperature increase in the Rhine basin as HadRM2, while in HadRM3H-B2 the increase is about 1.5°C lower. In the HadRM2 experiment the warming over the Alps is about 1° C more than that over the middle and lower part of the basin, whereas the warming is rather evenly distributed over the basin in the HadRM3H simulations. The largest warming occurs in the winter season in the HadRM2 experiment and in the summer season in the HadRM3H simulations. The relatively large increase in the mean winter temperature in the HadRM2 experiment is due to an increased southerly flow in the future climate (UKCIP, 2002), bringing warm air into the Rhine basin. The very large summer warming in the HadRM3H-A2 simulation is accompanied by a large reduction in precipitation and soil moisture. This increased summer dryness is considered further below. In all seasons, the warming is considerably larger than the corresponding bias of the control climate simulation reported in section 3.2, even at sub-basin scales.

b. Temperature variability

Table 5 presents changes in variability of temperature. In all experiments, the standard deviation of the 10-day temperature decreases in winter and increases in the other seasons. A similar seasonal pattern of the changes in variability in mid-latitude regions has been found in other regional climate model runs for daily (Mearns et al., 1995) and monthly (Gallardo et al., 2001) temperatures. The significance of the change in standard deviation was tested with a jackknife statistic of Beersma and Buishand (1999). In all experiments, changes in winter are highly significant and similar in magnitude (–17%). In summer, however, the HadRM2 and HadRM3H-A2 simulations give much stronger (≈30%) changes in standard deviations of temperature compared to the HadRM3H-B2 simulation (12%).

Table 5. Changes in the standard deviations of the 10-day mean temperatures in the HadRM2 and HadRM3H climate change experiments, expressed in terms of the ratios of standard deviations. The variances were averaged over the nine 10-day periods of the season and over all grid boxes in the Rhine basin. The figures in bold are significant at the 5% level.

	DJF	MAM	JJA	SON
σ ratio HadRM2-future/ control	**0.83**	1.04	**1.35**	**1.14**
σ ratio HadRM3H-future A2/control	**0.83**	**1.16**	**1.33**	1.02
σ ratio HadRM3H-future B2/control	**0.83**	1.11	1.12	1.08

c. Mean precipitation

Table 6 shows the simulated area-average precipitation changes under three forcing scenarios. The annual mean precipitation increases/decreases by about 4% in HadRM2/3H. In all experiments, there is an increase of precipitation in winter and a decrease in summer, with the largest changes in the HadRM3H-A2 experiment. The decrease in mean summer precipitation is even as large as 40% in that experiment. The HadRM2 experiment shows a rather strong increase (≈ 20%) in the mean autumn precipitation. By contrast, the mean autumn precipitation decreases in the HadRM3H simulations. In spring, the magnitude of changes is small (also between experiments). The changes in the seasonal mean precipitation are rather evenly distributed over the basin in the HadRM3H simulations. There is somewhat more spatial variation in these changes in the HadRM2 experiment. The decrease in mean summer precipitation is larger in the Alps (up to 29%) than in the rest of the basin, and a few grid boxes in the Alps also show a decrease in mean winter and spring precipitation in that experiment.

On average, the magnitude of the projected precipitation change is smaller than the bias of the control climate simulation for winter and spring. In summer, however, the projected changes are much larger than the bias even at sub-basin scales.

Table 6. As in Table 4 but for the percentage changes in precipitation.

	DJF	MAM	JJA	SON	Year
HadRM2	7.5	9.1	–14.7	+18.6	+4.5
HadRM3H-A2	24.9	4.1	–38.5	–13.7	–4.4
HadRM3H-B2	18.0	3.3	–27.5	–11.8	–3.5

d. Precipitation variability

Table 7 shows the changes in the coefficient of variation of the 10-day precipitation totals for the four seasons. In all experiments, the *CV* of precipitation increases in summer and this change is highly significant. In winter, *CV* significantly increases in the HadRM2 experiment, and significantly decreases in the HadRM3H simulations.

An increase in the *CV* of the 10-day precipitation totals can occur if (1) the day-to-day persistence increases, (2) the frequency of dry days increases, or (3) the coefficient of variation of the wet-day precipitation amounts increases (Räisänen, 2002). A large part of the changes in Table 7 can be attributed to changes in the frequency of dry days. In winter, both

Table 7. Same as in Table 5, but for the coefficient of variation *CV* of the 10-day precipitation amount.

	DJF	MAM	JJA	SON
CV ratio HadRM2-fut/cont	**1.25**	**1.14**	**1.28**	0.98
CV ratio HadRM3H-fut A2/cont	**0.84**	1.03	**1.43**	**1.18**
CV ratio HadRM3H-fut B2/cont	**0.88**	0.95	**1.33**	1.07

the number of dry days and the *CV* of the 10-day precipitation totals increase in the HadRM2 experiment, whereas these two quantities decrease in the HadRM3H simulations. The decrease in the mean summer precipitation is accompanied by an increase in the number of dry days, resulting in an increase in the *CV* of the 10-day precipitation totals. This is consistent with the results of Räisänen (2002) for the changes in *CV* of monthly precipitation in global climate model simulations. The largest increases in *CV* were found in areas with decreasing mean precipitation. Decreases in *CV* were found in high northern latitudes for seasons with a relatively large increase in mean precipitation.

e. Potential evaporation

Figure 5 shows that the calculated E_p from the HadRM3H-A2 output roughly doubles in the future climate. The large increase in summer potential evaporation is mainly the result of the increased summer dryness. Both the mean relative humidity and the mean cloud cover decrease by about 30% in summer. In particular, the change in relative humidity has a large impact on E_p.

The use of the Penman-Monteith equation to calculate potential evaporation under dry summer conditions has been questioned, see e.g. de Bruin (1987). Potential evaporation should in fact be based on weather variables over a well-watered vegetation rather than a vegetation suffering from limited soil water supply as simulated by HadRM3H in summer. For some 10-day periods, the average E_p is as large as 15 to 20 mm/day, corresponding to a heat flux of 450 to 600 W/m^2. These values should be considered as unrealistic.

f. Conclusions

The HadRM2 and HadRM3H-A2 experiments show both an increase in the annual mean temperature of about 4.5 °C over the Rhine basin by the end of the 21st century. There are, however, differences regarding the changes in seasonal mean temperature and precipitation. The HadRM3H-A2 experiment shows a strong decrease in mean summer precipitation (≈ 40%), which is accompanied by a relatively large temperature increase (≈ 6 °C) and a large increase in potential evaporation. By contrast, the largest temperature increase in the HadRM2 experiment is found in winter (≈ 6 °C). Mean autumn precipitation increases in the HadRM2 experiment (≈ 20%), but it decreases in the HadRM3H-A2 simulations (≈ 15%). Besides the differences between the changes in the seasonal mean precipitation, there are differences regarding the changes in the *CV* of the 10-day precipitation amounts.

The changes in the HadRM3H-B2 experiment show the same seasonal pattern as those in the A2 experiment, but are generally smaller (for the mean temperature and precipitation about 2/3 of those in the A2 experiment). For the application with the RhineFlow model, only the more extreme HadRM3H-A2 experiment was considered further.

4. River discharges from the HadRM3H control run

The output of global climate models has seldom been used as an input into hydrological models because of their coarse spatial resolution. The availability of regional climate model simulations largely meets this objection, particularly for large river basins that are covered by many grid boxes. Biases in these regional climate simulations may, however, have a strong impact on the simulated river discharges. For instance, the bias of 0.65 mm/day from Table 2 for the HadRM3H data leads to an additional discharge of 1200 m^3/s at Lobith ($\approx$ 50 % of the long-term annual mean discharge) when it is entirely translated into runoff. It is therefore not surprising that the RhineFlow model does not give realistic discharge data when it is fed directly with HadRM3H data without any correction. Figure 6 shows that the direct use[4] of the data from a 30-year control run yields an average discharge as high as 4000 m^3/s during winter and early summer.

Considering the sensitivity of the hydrological model to the precipitation input it is clear that a bias correction must be used to get meaningful output. For each gid box the simulated 10-day precipitation totals $P_{\mathrm{cont}}(t)$ were scaled by the ratio between the long-term means $\overline{P}_{\mathrm{obs}}$ and $\overline{P}_{\mathrm{cont}}$ of the observed and simulated precipitation amounts:

$$P_{\mathrm{cont,cor}}(t) = P_{\mathrm{cont}}(t) \times \overline{P}_{\mathrm{obs}} / \overline{P}_{\mathrm{cont}}, \quad t = 1,\ldots,36J \tag{1}$$

where J is the number of years (J = 30 for a single ensemble member and J = 90 for the concatenation of the three ensemble members). The means $\overline{P}_{\mathrm{obs}}$ and $\overline{P}_{\mathrm{cont}}$ were first calculated for each of the 36 periods of 10 days in the year and then smoothed using a Gaussian filter of seven 10-day periods to reduce the effect of sampling variability. The bias correction is the same for the three ensemble members ($\overline{P}_{\mathrm{cont}}$ is the average value of these members).

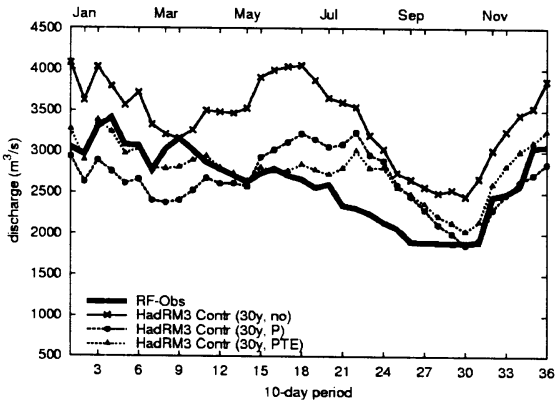

Figure 6. Mean discharge at Lobith for the 36 periods of 10 days in the year as simulated by RhineFlow with observed data (solid line) and with a 30-year HadRM3H control run: without bias correction (crosses), with bias correction in precipitation (dots), and with bias correction in precipitation, temperature and evaporation (triangles).

[4] For each 3 km × 3 km grid box of the RhineFlow model, the simulated temperatures were adjusted for the differences in altitude, using a lapse rate of 5.7 °C per km. No other adjustments were made.

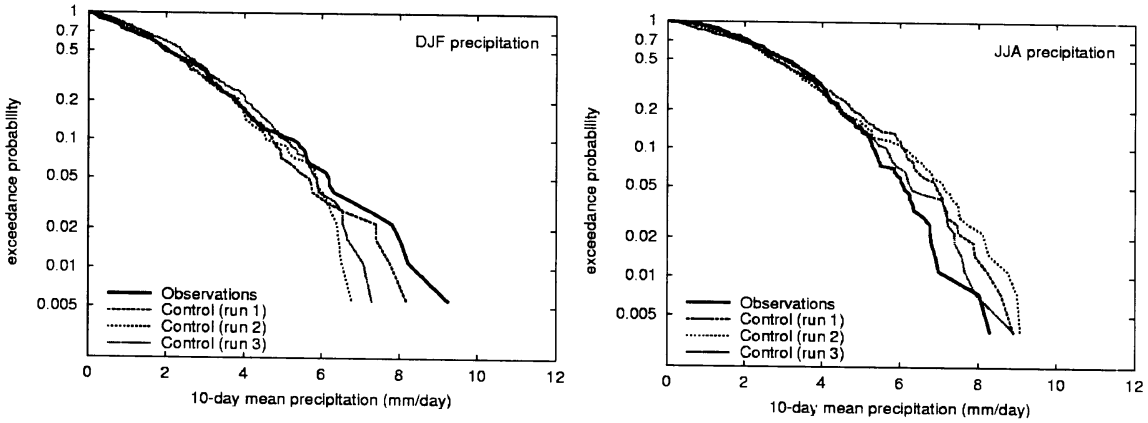

Figure 7. Exceedance probabilities of 10-day mean amounts for the observed precipitation and the bias-corrected precipitation in the HadRM3H simulations. The exceedance probabilities refer to the 10-day field averages in the winter (DJF, left panel) or summer (JJA, right panel) season.

Figure 7 shows the exceedance probabilities of the simulated basin-average 10-day precipitation totals after bias correction. Apart from some departures regarding the occurrence of large 10-day precipitation events (with 6 mm/day or more), there is a good correspondence with the exceedance probabilities for the observations. A similar result was achieved by Frei et al. (2003) with a simple bias correction of daily precipitation in regional climate model simulations.

From Figure 6 it can be seen that the bias reduction of precipitation leads to a much more realistic simulation of the mean annual discharge. However, the annual cycle is completely off, with the largest discharge in summer and relatively low discharges in winter. Qualitatively, the seasonal course of the sign of this bias agrees with that of the difference between the values of the potential evaporation in Figure 5. In winter, the values from the HadRM3H output are larger than those from the observed data, whereas in spring and early summer the HadRM3H values are smaller. This bias in potential evaporation was corrected in the same way as that in precipitation. In addition, the simulated temperatures were corrected with the difference between the observed mean temperature $\overline{T}_{\text{obs}}$ and the simulated mean temperature $\overline{T}_{\text{cont}}$:

$$T_{\text{cont,cor}}(t) = T_{\text{cont}}(t) + (\overline{T}_{\text{obs}} - \overline{T}_{\text{cont}}), \quad t = 1,\ldots,36J \tag{2}$$

Figure 6 shows that the mean winter discharge is close to the reference discharge after these corrections. The mean summer discharge remains, however, too high. So, apparently, forcing RhineFlow with correct mean values does not guarantee a correct mean response. This suggests a non-linear response to the meteorological input during (dry) summer conditions.

A further analysis showed that the bias is related to the correlation between E_p from HadRM3H and soil moisture in RhineFlow (plotted in Figure 8). For RhineFlow driven by observed meteorological data this correlation is –0.4, whereas RhineFlow driven by HadRM3H data gives –0.7. Since the actual evaporation is computed basically from the

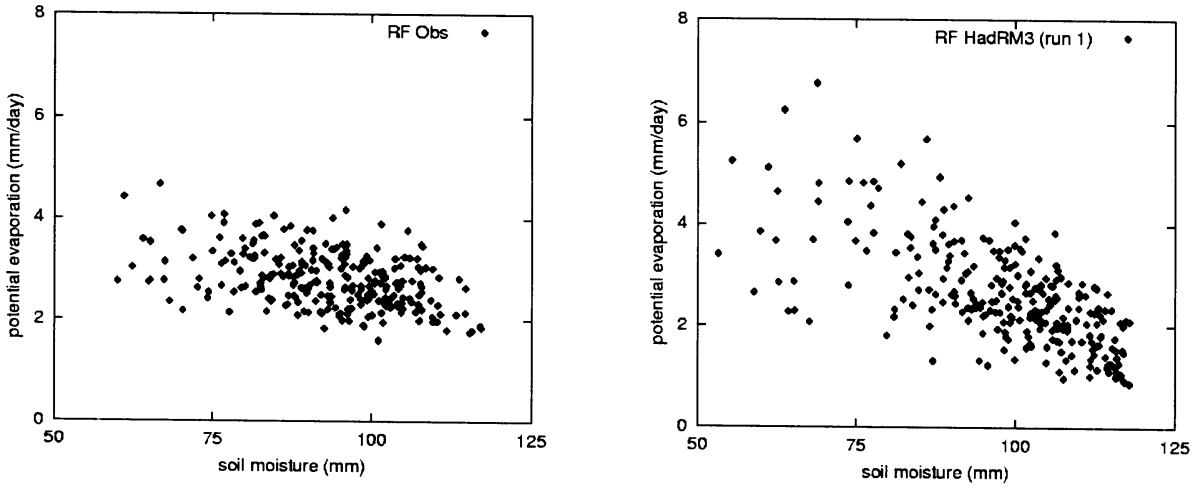

Figure 8. Scatter plots of potential evaporation against soil moisture as simulated by RhineFlow. In the left panel RhineFlow is driven by observed meteorological data, whereas in the right panel RhineFlow is forced with a 30-year bias-corrected HadRM3H control run. Shown are the 10-day field averages for the summer season (JJA).

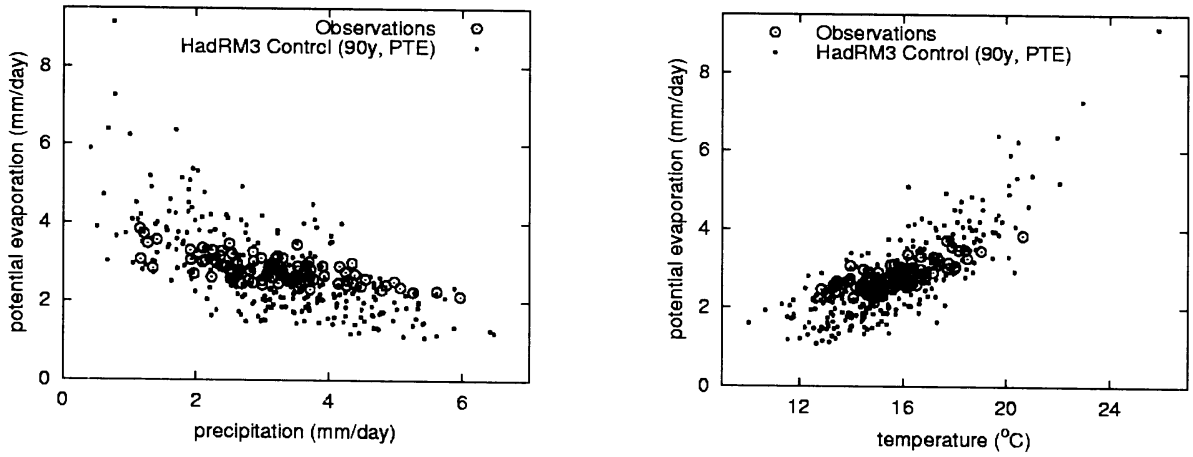

Figure 9. Scatter plots of potential evaporation against precipitation (left panel) and potential evaporation against temperature (right panel) for the observed data (circles) and bias- corrected HadRM3H control data (dots). Shown are the monthly field averages for the summer season (JJA).

product of E_p and normalized soil moisture (as a fraction of the soil moisture capacity), this correlation influences the 30-year mean actual evaporation. The relatively strong negative correlation for E_p from HadRM3H leads to a relatively low mean actual evaporation and an overestimation of the mean runoff in summer.

Furthermore, it turned out that the dependence of E_p on temperature as well as that of E_p on precipitation is too strong in the HadRM3H data. Figure 9 compares these dependencies for the observed monthly means and the bias-corrected monthly values of the HadRM3H control simulations. In the latter, extremely large values of E_p occur in months with low precipitation

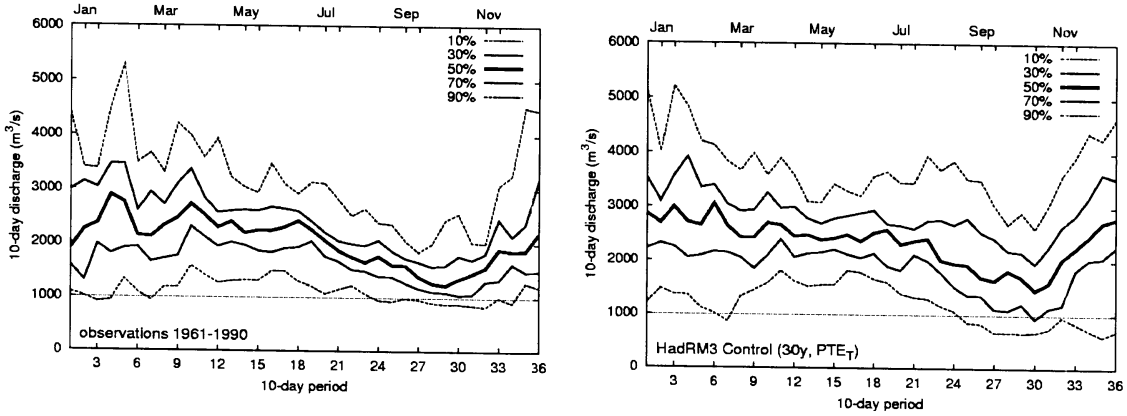

Figure 10. Quantiles of the 10-day flows at Lobith for each of the 36 periods of 10 days in the year. Shown are the 10, 30, 50, 70 and 90% quantiles from RhineFlow simulations with observed data (left panel) and a bias-corrected 30-year HadRM3H control run (right panel).

and high temperature. Also striking is the much larger temperature variability in the HadRM3H data. The warmest summer month in the HadRM3H data (26 °C) is about 5 degrees warmer than the maximum in the observations.

These results all point at a too strong hydrological feedback in the HadRM3H simulations. Dry conditions lead to a significant reduction in cloud cover, resulting in too high temperatures and reduced precipitation. Thus dry conditions in HadRM3H are to a rather high extent self-sustaining, and the same holds for wet conditions.

Because of the difficulties with the E_p values from the Penman-Monteith equation, it was decided to derive the potential evaporation for the HadRM3H simulations from temperature only, using a regression between the reference evaporation E_r and temperature for the observed climate. Details of this regression can be found in Appendix A. With this new estimate of E_p, the mean summer discharge decreased by about 500 m^3/s, cancelling the observed overestimation in Figure 6. There remains, however, a too strong persistence of dry and wet conditions in the HadRM3H simulations. As a result, the variability of the simulated flows is not entirely realistic in summer. The 10% and 90 % quantiles in Figure 10 show an increasing spread with time during summer using HadRM3H, in contrast to the decreasing spread in the simulation with observed meteorological data. The overestimation of the occurrence of high precipitation amounts in the HadRM3H data (Figure 7) also contributes to the bias in the variability of the summer discharge.

5. River discharges in future climates

5.1. Scenario construction

From the HadRM2 experiment two different scenarios were constructed to study the effect of the inclusion of the changes in the temperature and precipitation variability as presented in section 3.3. Both scenarios were obtained by modifying the observed data. In contrast, for the HadRM3H-A2 simulations the direct use of the bias-corrected model output was compared with a simple scenario based on perturbation of the 10-day temperature and precipitation in the control run.

The HadRM2 scenarios

For each HadRM2 grid box and for each of the 36 periods of 10 days in the year, the following quantities were computed: the 20-year averages of temperature $\overline{T}_{\text{fut}}$ and precipitation $\overline{P}_{\text{fut}}$ from the HadRM2 perturbed climate run, the 20-year averages $\overline{T}_{\text{cont}}$ and $\overline{P}_{\text{cont}}$ from the control climate run, the standard deviations of the 10-day temperatures σ_{fut} and σ_{cont}, and the CV of the 10-day precipitation amounts in the perturbed and control climate run of HadRM2. To reduce the effect of sampling variability, these quantities were smoothed using running means of seven 10-day periods. The changes in the smoothed quantities were applied to the 3 km × 3 km RhineFlow grid using a nearest-neighbour approach.

In the HadRM2 scenario 1, the difference $\overline{T}_{\text{fut}} - \overline{T}_{\text{cont}}$ is added to the 1961-1995 baseline series $T_{\text{obs}}(t)$ to form the scenario temperature series $T_{\text{scen}}(t)$:

$$T_{\text{scen}}(t) = T_{\text{obs}}(t) + (\overline{T}_{\text{fut}} - \overline{T}_{\text{cont}}), \quad t = 1,\ldots,36J \tag{3a}$$

where $J = 35$. This changes the mean of $T_{\text{obs}}(t)$, but has no effect on the variance. For precipitation, the ratio $\overline{P}_{\text{fut}} / \overline{P}_{\text{cont}}$ is applied to the baseline series $P_{\text{obs}}(t)$:

$$P_{\text{scen}}(t) = P_{\text{obs}}(t) \times \overline{P}_{\text{fut}} / \overline{P}_{\text{cont}}, \quad t = 1,\ldots,36J \tag{3b}$$

This transformation has the effect of changing the mean of $P_{\text{obs}}(t)$ by that ratio, but also changes the variance by the ratio squared; CV remains, however, unchanged, as already noted in section 3.2.

In the HadRM2 scenario 2, the HadRM2-projected changes in the mean and variance of the 10-day temperatures are accounted for by using the following linear transformation of $T_{\text{obs}}(t)$:

$$T_{\text{scen}}(t) = [T_{\text{obs}}(t) - \overline{T}_{\text{obs}}] \times \sigma_{\text{fut}} / \sigma_{\text{cont}} + \overline{T}_{\text{obs}} + (\overline{T}_{\text{fut}} - \overline{T}_{\text{cont}}), \quad t = 1,\ldots,36J \tag{4}$$

Here $\overline{T}_{\text{obs}}$ stands for the 35-year averages of the observed 10-day temperatures (36 values). This transformation changes the mean of $T_{\text{obs}}(t)$ as in HadRM2 scenario 1, but also changes the standard deviation of $T_{\text{obs}}(t)$ by the ratio $\sigma_{\text{fut}} / \sigma_{\text{cont}}$.

A similar transformation as (4) for precipitation to account for the increase in CV results in negative values of $P_{\text{scen}}(t)$ for a number of 10-day periods. Simple replacement of these negative values by zeros increases the mean additionally by about 4%. To avoid these negative values, Weibull distributions were fitted to the observed 10-day precipitation amounts (36 different distributions for each grid box). The estimated parameters of these distributions were then modified according to the changes in the mean and CV in the HadRM2 experiment. Finally, new precipitation values were computed with the modified parameters. Details of the HadRM2 precipitation scenario 2 can be found in Appendix B.

In both HadRM2 scenarios potential evaporation was obtained by multiplying the values for the baseline period with a factor determined by the simulated change in mean temperature, $\overline{T}_{\text{fut}} - \overline{T}_{\text{cont}}$ (section 3.1).

a. The HadRM3H scenarios

Apart from a simple scenario based on the perturbation of the data for present-day conditions (HadRM3H scenario 1), the direct use of the bias-corrected output of the HadRM3H-A2 simulations was considered (HadRM3H scenario 2). The HadRM3H scenario 1 was obtained by perturbing the bias-corrected 10-day temperature and precipitation in the three control simulations for the period 1961-1990:

$$T_{\text{scen}}(t) = T_{\text{cont,cor}}(t) + (\overline{T}_{\text{fut}} - \overline{T}_{\text{cont}}), \quad t = 1,\ldots,36J \tag{5a}$$

$$P_{\text{scen}}(t) = P_{\text{cont,cor}}(t) \times \overline{P}_{\text{fut}} / \overline{P}_{\text{cont}}, \quad t = 1,\ldots,36J \tag{5b}$$

An advantage of perturbing the control climate rather than the observed climate is a longer baseline period ($J = 90$ years). The use of the control climate was also desirable to make the comparison with the HadRM3H scenario 2 as clean as possible. For both HadRM3H scenarios, 10-day values of potential evaporation were derived from the 10-day temperatures as discussed in Appendix A. To investigate the sensitivity to the changes in potential evaporation a low (L), middle (M) and high (H) scenario were formulated. In the low scenario there is no change in potential evaporation, whereas in the middle scenario the change in potential evaporation is comparable to that in the HadRM2 scenarios. The emphasis is therefore on the middle scenario.

The changes in the seasonal mean temperature, precipitation and potential evaporation in the HadRM3H scenario 1 are the same as those in the HadRM3H scenario 2. Differences occur with respect to the variability of precipitation and temperature and the shape of their distributions in the future climate.

The temperatures were corrected for the differences in altitude between the RhineFlow and HadRM3H grid boxes, using a lapse rate of 5.7 °C per km. The precipitation of each RhineFlow grid box was the same as that of the corresponding larger HadRM3H grid box.

5.2. Changes in seasonal flows

a. Changes from the HadRM2 scenarios

Figure 11 presents the annual cycle of the mean10-day flows in the RhineFlow simulations with the HadRM2 scenarios and in the RhineFlow simulation for the present-day climate. Two gauging stations are considered: Rheinfelden in Switzerland and Lobith in the Netherlands (Figure 1). There is little difference between the changes predicted by the two scenarios. The relative changes from HadRM2 scenario 1 are shown in Figure 12.

While the mean annual flow does not change much, there is a marked redistribution of discharge within the year. For Lobith the annual cycle becomes more pronounced as a result

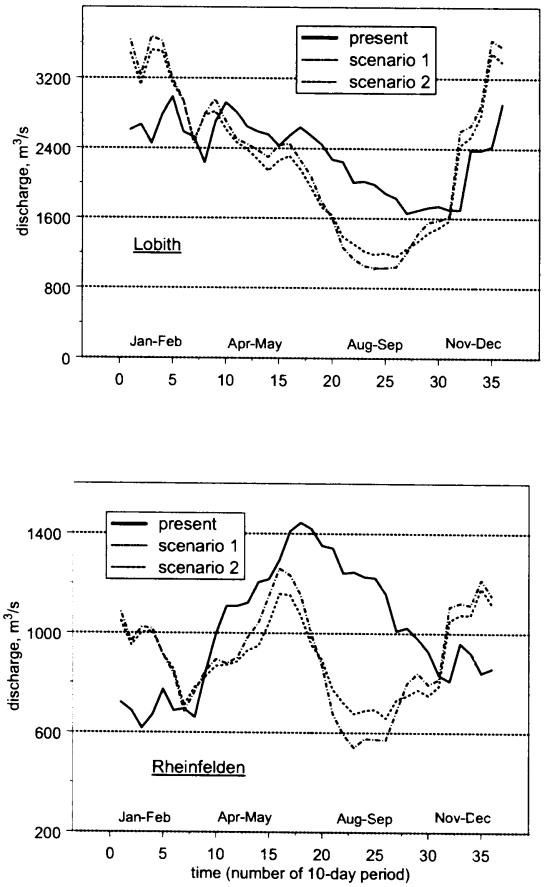

Figure 11. Mean discharge at Lobith and Rheinfelden for the 36 periods of 10 days in the year as simulated by RhineFlow with observed data (present climate) and with the HadRM2 scenarios 1 and 2 for the future climate.

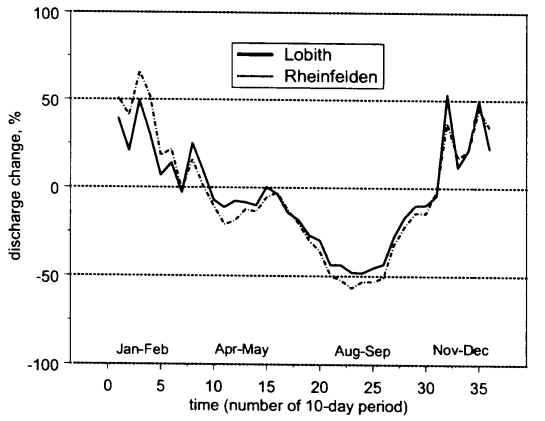

Figure 12. Relative change (%) in the mean discharge at Lobith and Rheinfelden for each of the 36 periods of 10 days in the year as obtained from RhineFlow driven by HadRM2 scenario 1.

Table 8. Percentage changes in some components of the water balance in the Rhine basin under HadRM2 scenario 1. Shown are annual and seasonal averages over the area upstream of the indicated station.

Station	Discharge (%)			Actual evaporation (%)			Soil moisture (%)		
	Year	DJF	JJA	Year	DJF	JJA	Year	DJF	JJA
Lobith	–3.4	28.9	–30.6	12.9	24.5	1.2	–6.2	0.2	–12.2
Maxau	–6.0	30.2	–33.9	20.2	29.6	13.2	–2.3	–0.2	–4.7
Rheinfelden	–4.6	37.4	–34.7	27.5	46.3	15.8	–1.6	0.0	–3.4

of an increase in the mean 10-day flows in winter (up to about 3500 m^3/s) and a decrease of the mean flows in summer (down to about 1100 m^3/s). The summer peak in the flow at Rheinfelden is strongly reduced and there is no longer a minimum during winter at this gauging station in the HadRM2 scenarios. These results are in qualitative agreement with scenario discharges for the Rhine in earlier studies of Kwadijk and Rotmans (1995) and Middelkoop (2000).

Table 8 shows the changes in the annual and seasonal means for a number of water balance components of the Rhine basin. Shown are averages over the areas upstream of Lobith, Maxau and Rheinfelden. During winter the discharge increases by about 30 % in Lobith and Maxau, and by 37% in Rheinfelden. The increase in mean winter discharge is due to the increase of precipitation and the fact that warming leads to a decrease in the amount of precipitation that is stored as snow and to an increase in early melt. During summer the discharge of the Rhine decreases by about 30% in Lobith and by about 35% in Rheinfelden. In August, the reduction of discharge is even as large as 50% (Figure 12). This is in line with the decreased summer precipitation and, in the Alps, with the increased evaporation. Also, due to the general decrease of snow storage in the Alps, the input from snowmelt in the early summer decreases. Note that the actual evaporation over the entire river basin hardly changes, because of decreasing soil moisture. The 1 % increase in mean actual evaporation in the RhineFlow simulations during summer corresponds quite well with a decrease of 3 % found in the direct climate model output.

b. Changes from the HadRM3H scenarios

Figure 13 presents the annual cycles of five quantiles of the 10-day flows at Lobith for the RhineFlow simulations with the HadRM3H scenarios. The median (50% quantile) shows a clear annual cycle, which is comparable to that in Figure 11 for the mean from the HadRM2 simulations and is also the result of an increase in the winter flows and a decrease in the summer flows. Though the medians of the winter flows are almost the same for the two HadRM3H scenarios, the interquantile differences are larger for the HadRM3H scenario 1. The larger spread for this scenario is due to the fact that it does not account for the decrease in the *CV* of the 10-day precipitation totals in winter (Table 7). The situation is reversed in summer: the spread is then smaller for the HadRM2 scenario 1. It should be stressed again that the changes in mean temperature, precipitation and potential evaporation are the same in both scenarios.

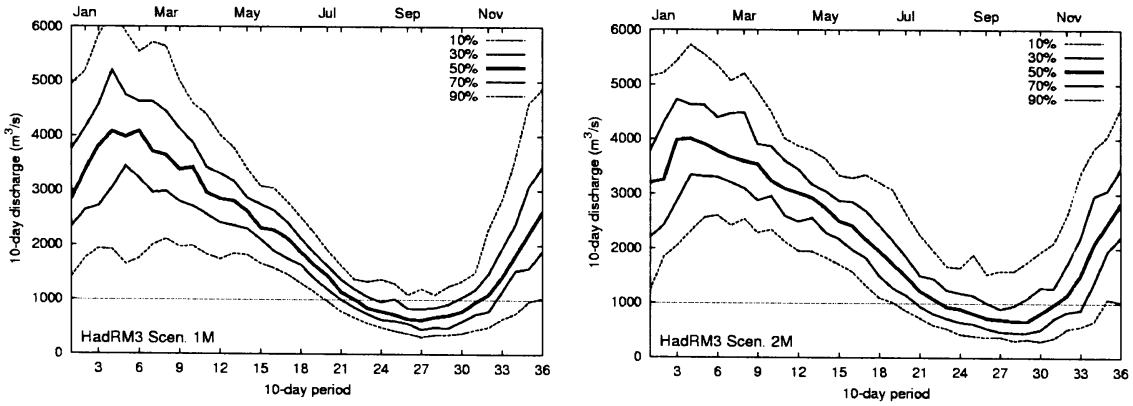

Figure 13. Quantiles of the 10-day flows at Lobith for each of the 36 periods of 10 days in the year. Shown are the 10, 30, 50, 70 and 90% quantiles from RhineFlow simulations with the HadRM3H scenario 1 (left panel) and HadRM3H scenario 2 (right panel) for the future climate.

Figure 14 shows the relative changes in the 10-day mean discharge at Lobith for the bias-corrected climate model output data (HadRM3H scenario 2) with a low, middle and high scenario for the change in potential evaporation. Compared with the relative changes in the HadRM2 scenario 1 in Figure 12, the period with a considerable decrease in the mean discharge lasts longer in the HadRM3H scenario. The choice of the evaporation scenario has limited influence on the decrease in the mean summer flows. This is because the actual evaporation is reduced earlier in a scenario with a relatively high potential evaporation. An interesting point is that the choice of the evaporation scenario has some influence on the change in the mean winter discharge because of the memory of the soil water and groundwater storages in the hydrological model.

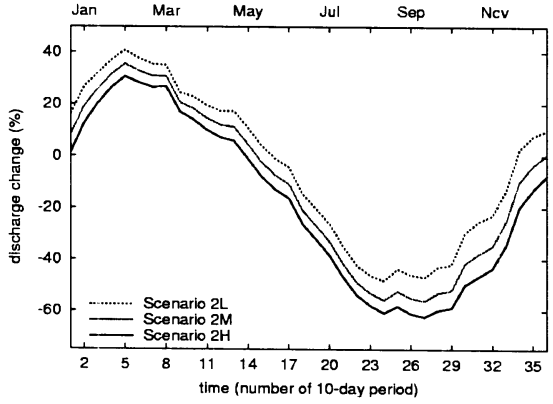

Figure 14. Relative change (%) in the mean discharge at Lobith for each of the 36 periods of 10 days in the year as obtained from RhineFlow driven by HadRM3H scenario 2 with a small (L), intermediate (M) and large (H) change in potential evaporation.

5.3. Changes in annual maximum flows

Climate-induced changes in the distribution of the annual maximum flows may have strong impacts on flood protection. For the non-tidal part of the Rhine in the Netherlands flood-protection works have to withstand a discharge that is exceeded on average once in 1250 years. Traditionally this design discharge has been based on a statistical analysis of the 1-day annual maximum flows at Lobith. The RhineFlow model, however, provides only the 10-day flows. The question how far the change in the 1-day annual maximum flows can differ from that in the 10-day annual maxima is therefore addressed first. Then the changes in the annual maximum flow distribution from the HadRM2 and HadRM3H scenarios are presented and compared with those in Middelkoop (1999). Finally, an uncertainty analysis is given for the changes in the HadRM3H scenarios, based on the bootstrap.

a. 1-day versus 10-day annual maximum flows

For each water year, the largest 1-day and 10-day flows were extracted from the daily flow record of Lobith for the period 1901-2000 (99 water years). It emerged that the 1-day annual maximum flow is on average 28 % larger than the 10-day annual maximum flow. The relative difference is somewhat larger (31%) if only the 10 largest annual maximum flows are considered. Because of the interest in extremely high flows, the potential change in this relative difference is examined further.

When the daily flows are multiplied by a constant factor, then the 1-day and 10-day annual maximum flows change with the same factor, and their relative difference obviously remains unchanged. This is no longer true if the daily flows are modified by the power transformation:

$$Y = X^{\theta} \tag{6}$$

This transformation was applied for $\theta = 0.75, 0.80, \ldots, 1.5$. For each θ, the 1-day and 10-day annual maximum flows and the CV of the 10-day average flows were determined. The latter was averaged over the period 1 November till 1 April, in which most high river flows are found. This average CV is denoted as $\overline{CV}_{\theta}$, and the ratio between the averages of the 10 largest 1-day and 10-day annual maximum flows as r_{θ}. The relationship between these two quantities is almost linear:

$$r_{\theta} \approx 1.024 + 0.289 \times \overline{CV}_{\theta} / \overline{CV}_{0} \tag{7}$$

Note that for $\theta = 0$ (no change in the daily flows), $r_0 = 1.313$, in agreement with the 31% mentioned above. For $\theta > 1$, both CV and the ratio between the 1-day and 10-day annual maximum flows increase. A relative increase in the CV of 20% (about the increase in the HadRM2 scenario 2) results in $r_{\theta} = 1.371$, which is only 4% larger than r_0. The relative change in a quantile of the distribution of the 1-day annual maximum flows will therefore not differ much from that in the corresponding quantile of the 10-day annual maximum distribution.

b. Changes from the HadRM2 scenarios

The 10-day annual maximum flows, $Q_{\max}$, of the discharge series are described here by the Gumbel distribution that takes the form:

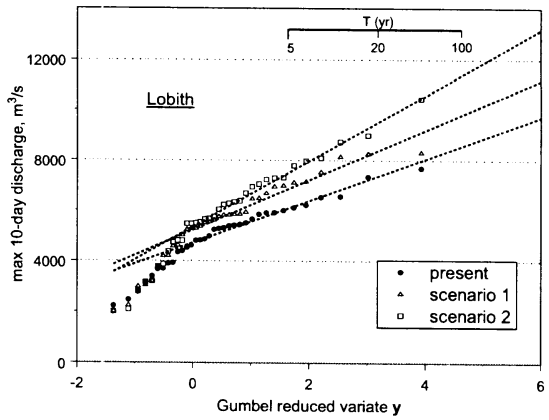

Figure 15. Gumbel plot of the 10-day annual maximum flows at Lobith in the RhineFlow simulations with observed data (present climate) and with the HadRM2 scenarios 1 and 2 for the future climate. The straight lines show the maximum likelihood fits of the Gumbel distribution to the samples censored at the 20th largest value.

$$F(x) = \Pr(Q_{\max} \le x) = \exp\{-\exp(-(x-\xi)/\alpha)\}, \tag{8}$$

where ξ is the location parameter and α the scale parameter of the distribution. The mean return period T of an exceedance of a value x follows from $T = 1/[1\text{-}F(x)]$.

Figure 15 shows a Gumbel plot of the annual maxima of the simulated 10-day flows for present-day conditions, using observed meteorological data, and for the two HadRM2 scenarios. If these annual maxima came from a Gumbel distribution, they would follow a straight line. Figure 15 shows that this does not apply to the lower tail of the distribution. The straight lines in the figure are based on the maximum likelihood estimates of the parameters ξ and α for the sample censored at the 20th largest value of $Q_{\max}$ (Harter and Moore, 1968). From the figure it can be seen that the quantiles of the annual maximum distribution increase in the future climate, in particular in the HadRM2 scenario 2 that accounts for the increase in the CV of precipitation. This large impact of the change in variability on extreme flows is in line with results of Prudhomme et al. (2002) for the Severn catchment (UK). These authors constructed three scenarios from the output of the HadCM2 global climate model: a scenario similar to the HadRM2 scenario 1 by applying the relative changes in monthly mean precipitation to the observed daily data, a scenario in which the changes in monthly mean precipitation were achieved by modifying the number of wet days in the observed data (resulting in wetter winter months with more wet days and drier summer months with more dry days), and a scenario in which the changes in monthly mean precipitation were achieved by adjusting only the largest observed daily precipitation amounts. The change in the flood frequency distribution strongly depended on the scenario used.

Table 9. Relative change (%) in the quantiles of the flows at Lobith in different scenarios for the end of the 21st century.

Return period T (years)	HadRM2 scenario		UKHI2100 scenario
	1	2	
10	13	26	40
100	15	33	40
1000	15	37	25

Table 9 compares the relative increase in a number of extreme quantiles for the two HadRM2 scenarios with that in an earlier study of Middelkoop (1999). The latter was based on the output of the UKHI general circulation model of the Hadley Centre. The temperature increase in the UKHI2100 scenario of Middelkoop (4 °C) is comparable to that in the HadRM2 scenarios (Table 4). The UKHI2100 scenario shows a larger increase in precipitation, which leads to a relatively large increase in the 10-year and 100-year events in Table 9 for this scenario. The largest increase in the 1000-year event[5] is, however, found for the HadRM2 scenario 2, partly because it is the only scenario with an increase in the CV of precipitation. The change in the 1000-year event is also sensitive to the statistical method used to estimate this extreme event. The values for the HadRM2 scenarios were obtained by extrapolating the fitted Gumbel distribution in Figure 15. The value for the UKHI2100 scenario is based on the conditional peak method of Kwadijk and Middelkoop (1994). This method makes use of the relation:

$$\Pr(Q_p > x) = \int_0^\infty \Pr(Q_p > x \mid Q_{10d} = y) f_{10d}(y)\,dy \qquad (9)$$

with Q_p the largest daily flow in a 10-day period, Q_{10d} the average flow in that 10-day period, and $f_{10d}(y)$ the probability density (pdf) of Q_{10d}. For a flood peak Q_p as large as the 1000-year event, the result is sensitive to the values of $\Pr(Q_p > x \mid Q_{10d} = y)$ and $f_{10d}(y)$ for large y, in particular for y beyond the range of the observed 10-day average flows. Kwadijk and Middelkoop (1994) and Middelkoop (1999) approximated the pdf of Q_{10d} by a histogram and used the lognormal distribution to describe the distribution of Q_p for each class of this histogram. The observed drop in the relative change of the quantiles[6] from 40% for $T = 100$ year to 25 % for $T = 1000$ year in Table 9 could be an artefact due to their coarse approximation of the upper tail of the distribution of Q_{10d}.

The relative changes for the HadRM2 scenarios for $T = 100$ and $T = 1000$ years assume that the Gumbel distribution remains valid outside the range of the data both in the present-day and the future climate. There is an additional uncertainty in these relative changes due to the estimation of the parameters ξ and α from a record as short as 35 years. This uncertainty is quantified at the end of this section.

[5] For the sake of consistency with the study of Middelkoop (1999), the 1000-year event is given rather than the 1250-year event. For the HadRM2 scenarios the relative change in the 1250-year event is almost identical to that in the 1000-year event.

[6] The quantiles from the UKHI2100 scenario probably refer to the distribution of Q_p and not to the distribution of the annual maxima as in the case for the HadRM2 scenarios. For long return periods, the two different types of quantiles are almost identical provided that there is no clustering of large values of Q_p.

c. Changes from the HadRM3H scenarios

A Gumbel plot of the 10-day annual maximum flows for the HadRM3H control simulation and the two future HadRM3H scenarios is shown in Figure 16. The straight lines in the figure are based on a maximum likelihood fit to the data censored from below at 4000 m^3/s. There is a strong increase in the quantiles ($\approx$ 25% at moderate return periods) of the annual maximum distribution in the HadRM3H scenario 1. In contrast, there is only a modest increase ($\approx$ 10%) in the HadRM3H scenario 2 based on the direct model output. Table 10 compares the relative increase in a number of extreme quantiles. For the HadRM3H scenario 2 both the results for the middle and high scenario for the change in potential evaporation are given. This shows that the change in potential evaporation has little effect on the quantiles of the annual maximum distribution of the 10-day flows.

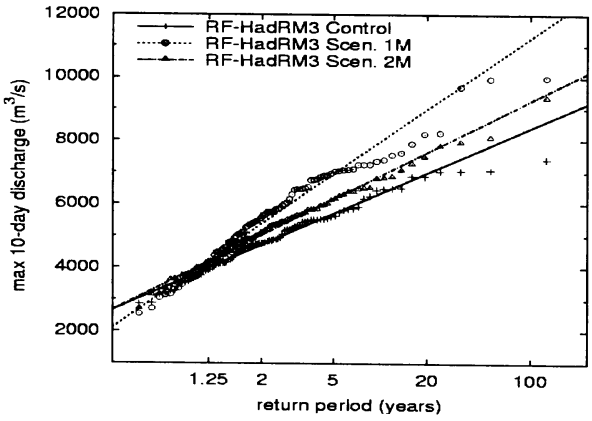

Figure 16. Gumbel plot of the 10-day annual maximum flows at Lobith in the RhineFlow simulations driven by the bias-corrected HadRM3H control simulation and by the HadRM3H scenarios 1 and 2 for the future climate. The straight lines show the maximum likelihood fits of the Gumbel distribution to the samples censored at 4000 m^3/s.

The differences between the HadRM3H scenarios 1 and 2 in Figure 16 and Table 10 demonstrate again that the changes in precipitation variability have a large influence on extreme flows. Figure 17 shows an estimated pdf and exceedance probabilities of the basin-average 10-day precipitation amounts in winter. In the HadRM3H scenario 1 there are more events with relatively high precipitation amounts (more than 5 mm/day) and a smaller number of events with low precipitation compared to the direct forcing approach. This is in line with

Table 10. Relative change (%) in the quantiles of the annual maximum distribution of the 10-day flows at Lobith in the HadRM3H scenarios (M indicates that the middle scenario for the change in potential evaporation was used, and H the high scenario).

Return period T (years)	HadRM3H scenario		
	1M	2M	2H
10	26	9	6
100	34	10	8
1000	39	11	10

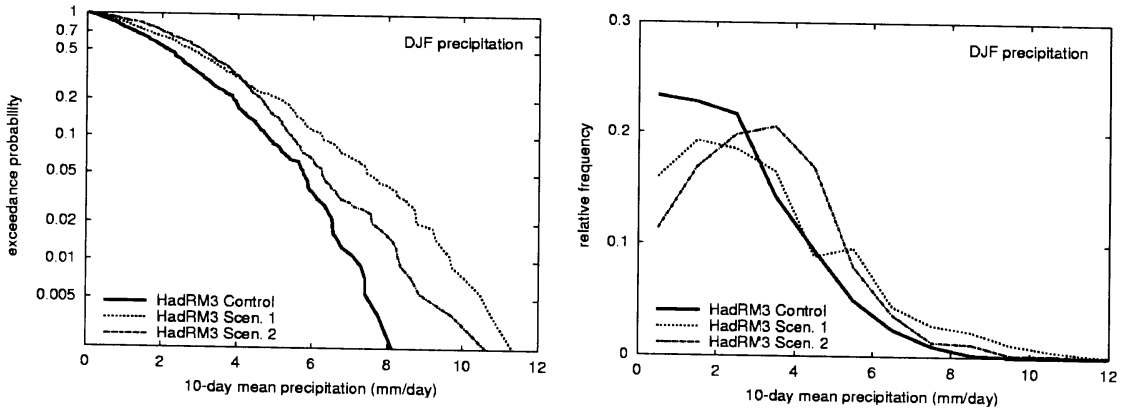

Figure 17. Probabilities of exceedance (left panel) and probability density (right panel) for the basin-average 10-day precipitation amounts in winter (DJF) in the HadRM3H control climate (solid line), HadRM3H scenario 1 (dotted line) and HadRM3H scenario 2 (dash-dotted line).

the decrease in *CV* of the 10-day precipitation amounts in winter in the HadRM3H simulations (Table 7). The relatively large increase in the high precipitation amounts in the HadRM3H scenario 1 leads to a relatively large increase in the upper quantiles of the distribution of the 10-day flows in winter (Figure 13). For the annual maximum flows this gives rise to a steeper slope of the Gumbel plot.

d. Estimating the uncertainty by the bootstrap

The accuracy of the estimated change of an extreme quantile depends on sample size. A larger sample of annual maximum flows leads to more accurate estimates of the parameters ξ and α of the underlying Gumbel distribution and reduces the uncertainty about the change in the quantiles of the distribution in the future climate. The bootstrap is a simple resampling technique to demonstrate this uncertainty.

In the case of time series perturbation (HadRM3H scenario 1) the weather of the future climate is connected to that of the present-day climate. In fact, the temperature and precipitation in the future climate from the linear transformation rules given by Eq. (5) are perfectly correlated with the temperature and precipitation in the control run. As a consequence, the annual maximum flows in the future and control climate will generally be positively correlated, which results in a more accurate estimation of the difference between the quantiles of their distribution compared to the situation that these annual maximum flows are independent. The latter is the case with the direct use of the climate model output (HadRM3H scenario 2). The bootstrap is capable of handling both the situation of dependent and independent annual maximum flows.

In the bootstrap method, J^* years are drawn with replacement from the 90 years of the control and future climate. To demonstrate the effect of sample size, J^* was taken 30 (length of a HadRM3H ensemble member) or 90. The 100-year event was estimated by fitting a Gumbel distribution to the annual maximum flows of these J^* years. This was done for both the

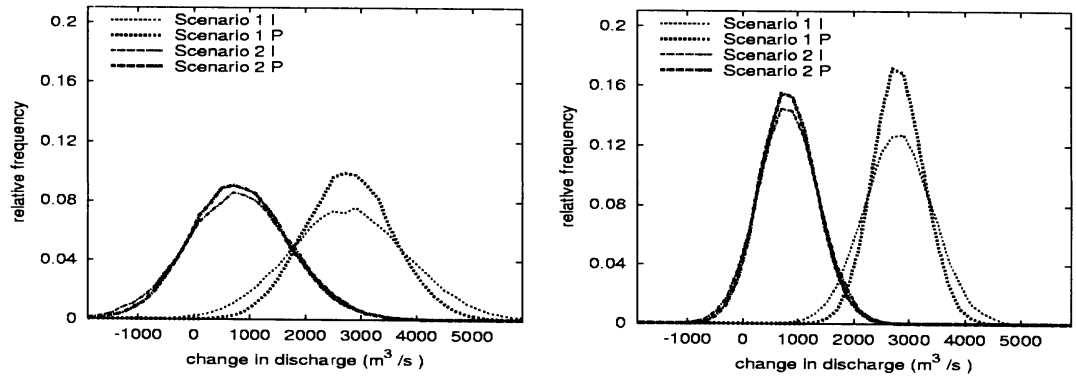

Figure 18. Frequency distributions of 20,000 bootstrap replications of the changes in the 100-year flood at Lobith from the HadRM3H scenario 1 (delta approach) and the HadRM3H scenario 2 (direct model output). Results are shown for bootstrap samples of 30 years (left panel) and 90 years (right panel). P indicates that paired annual maxima from the control and future climate were sampled, and I denotes that the bootstrap samples for the two climates are independent.

control and future climate, resulting in an estimate of the change in the 100-year event. The whole procedure was repeated B = 20,000 times to obtain a frequency distribution of possible changes of this event. This bootstrap experiment was done for both the annual maximum flows from the HadRM3H scenario 1 and those from the HadRM3H scenario 2. In addition, to investigate the influence of dependence between the annual maximum flows in the future and control climate, bootstrap samples were drawn from the paired annual maxima in the 90 years control and future climate and also from the annual maxima in the control and future climate separately.

Results of these experiments are shown in Figure 18. The direct forcing approach (HadRM3H scenario 2) gives a mean increase of about 900 m^3/s consistent with the Gumbel plot in Figure 16, and a broad band of uncertainty. For the 90-years sample the uncertainty is clearly smaller than for the 30-years sample. Though the 100-year event increases in most bootstrap samples, there is a significant probability of predicting a decrease, in particular with the smaller sample size. The independent and the paired results are close together, because the annual maximum flows in corresponding years of the control and future climate are basically independent. The perturbation of the control climate (HadRM3H scenario 1) leads to a larger mean increase (about 2800 m^3/s) than the direct forcing approach. The result of the paired resampling method is somewhat more peaked, but the difference with the independent resampling method is not very large. The reduction of the uncertainty in the change of the 100-year event due to dependence between the annual maximum flows in the future and control climate might not be interesting from a practical point of view.

From the bootstrap experiment it follows that the standard error of the change in the 100-year flow is about 500 m^3/s for both HadRM3H scenarios (J = 90), which is about 6% of the 100-year flow in the HadRM3H control climate. This figure for the relative standard error also applies for T = 10 and T = 1000 years in Table 10. For the HadRM2 scenarios in Table 9, the standard errors are about 50% larger, mainly because of the shorter scenario runs. It should be noted that these standard errors only account for the uncertainty due to the limited sample size

and not for the uncertainty about the underlying distribution and the differences between climate models.

e. Conclusion

The changes in the quantiles of the distribution of the annual maximum flows were studied for the HadRM2 and HadRM3H scenarios. The magnitude of these changes turned out to be very sensitive to the method of scenario construction. Because changes in variability have a large influence on the quantiles of the distribution of the annual maximum flows, it is generally not sufficient to use a simple perturbation of observed rainfall records or the control run of a climate model. For the most appropriate HadRM2 scenario, the 1000-year event increases by as much as 37%, partly as a result of a rather strong increase in the *CV* of the 10-day precipitation amounts in winter. The situation is quite different for the HadRM3H simulations where the *CV* of the 10-day precipitation amounts decreases in winter. The relative increase in the 1000-year event is only about 10% if the bias-corrected output of these simulations is used as a scenario.

5.4. Changes in low flows

The strong decrease in the mean summer discharges in the HadRM2 and HadRM3H scenarios suggests an increase in unfavourable conditions for inland navigation. Table 11 shows the proportion of 10-day periods that the Rhine discharge at Lobith is below a certain threshold. For the present climate, RhineFlow was driven by observed data in the HadRM2 scenarios and by the bias-corrected control simulations in the HadRM3H scenarios. The RhineFlow model was recalibrated after the application with the HadRM2 data (section 2.2), which resulted in a decrease in the frequency of low flows. River flows below 1000 m^3/s impose severe limitations on navigation in the Netherlands (Grabs, 1997). The number of 10-day periods that this occurs roughly doubles in the HadRM2 scenarios and quadruples in the HadRM3H scenarios compared to present-day conditions. The method of scenario construction has little influence on this frequency.

For the HadRM3H scenarios the additional costs for inland navigation resulting from the increased frequency of low flows were calculated using an empirical relationship between these costs and the discharge deficit from the "Drought Study of the Netherlands" (Droogtestudie Nederland, 2003). For each year, the accumulated monthly discharge deficit below 1250 m^3/s (denoted by D_{1250}) was calculated as

$$D_{1250} = \sum_{i=1,12} \max[1250 - D(i), 0], \tag{10}$$

Table 11. Proportion (%) of 10-day periods that the Rhine discharge at Lobith is below a certain threshold as simulated by RhineFlow.

Threshold (m^3/s)	HadRM2			HadRM3H		
	Present	Scenario 1	Scenario 2	Present	Scen 1M	Scen 2M
2300	56	58	61	44	58	52
1600	29	38	40	18	42	36
1000	8	16	18	5	24	22

with $D(i)$ the mean discharge in month i in m^3/s. It was observed that additional transport costs due to drought, C, are proportional to D_{1250}:

$$C = 0.3D_{1250} \qquad \text{Million Euros.} \tag{11}$$

Figure 19 presents a quantile plot of D_{1250} with the related additional transport costs on the right-hand side. Shown are results computed from observed discharges for the period 1901-2000 at Lobith and results for RhineFlow-3 driven by the bias-corrected control simulation of HadRM3H. There is a good correspondence between the observed and simulated D_{1250}. The additional transport costs are zero in an "average year" (50 % quantile), but once every 10 years (90 % quantile) costs exceed 300 Million Euros, and for the most extreme years costs amount up to 700 Million Euros or more.

For the future climate (2070-2099) the predicted discharge deficits and associated costs are much higher. Results are shown for the HadRM3H scenario 1 and HadRM3H scenario 2. For the latter a middle scenario (M) and a high scenario (H) for the change in potential evaporation are distinguished. Despite the differences between the scenarios, the general picture from these integrations is quite consistent. In almost every year additional costs are encountered. The additional transport costs in an "average year" are substantial, ranging from 450 to 600 Million Euros, and in extreme years these costs can amount to 1.0 Milliard Euros or more.

The average additional transport cost due to drought is in the present climate about 80 Million Euros a year. In the future climate these costs may increase to 480-550 Million Euros a year.

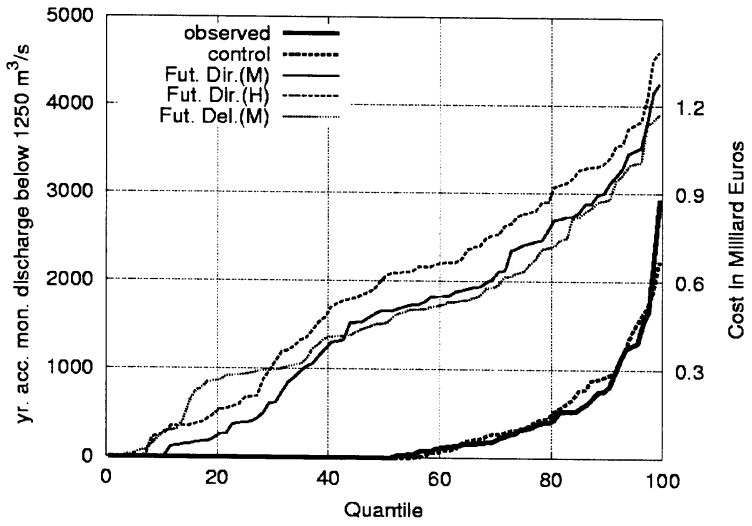

Figure 19. Quantiles of the yearly accumulated monthly discharge deficit below 1250 m^3/s at Lobith and of the estimated additional transport costs for inland navigation. Results are shown for RhineFlow simulations driven by observed data and bias-corrected HadRM3H data for the present climate and by three HadRM3H scenarios for the future climate: HadRM3H scenario 1M, HadRM3H scenario 2M, and HadRM3H scenario 2H, where M indicates the middle scenario for the change in potential evaporation, and H the high scenario.

The uncertainty of the cost estimates given above is quite large. They are based on regional climate model simulations with a rather strong decrease in summer precipitation. A large part of the summer discharge at Lobith (70% under present-day conditions) originates from precipitation and snow melt in the Alpine region. It is this region where the largest local bias corrections to precipitation were applied. Furthermore, RhineFlow-3 does not represent the low discharges very well. On the one hand, it overestimates the frequency of very low discharges (below any threshold < 1000 m^3/s). But, on the other hand, the frequency of discharges between 1000-1250 m^3/s is underestimated, which compensates for the first bias, leading to a surprisingly good correspondence between D_{1250} in the control simulation and the observed D_{1250}. The use of the empirical relation (11) does not account for changes in the number and types of ships due to economic and technical developments and adaptation to climate change.

6. Discussion and conclusions

The effect of climate change on the flow regime of the river Rhine was studied using the output of two regional climate models (HadRM2 and HadRM3H) from the Hadley Centre and a distributed water balance model (RhineFlow) of the river basin. From the output of each climate model two scenarios with a 10-day temporal resolution were constructed for the climate at the end of the 21st century.

For Lobith in the Netherlands, all scenarios result in an increase in mean winter discharge (20 – 30 %) and a decrease in mean summer discharge (30 – 40%). The increase in the winter discharge is caused by the increased precipitation in winter in combination with reduced snow storage and increased early melt. The decrease in the summer discharge is related to the decreased precipitation in summer and the reduction of snow melt from the Alps.

The larger mean discharges in winter lead to an increase of the quantiles of the distribution of the annual maximum flows. The magnitude of this increase turned out to be strongly dependent on the method of scenario construction, in particular the incorporation of the changes in the relative variability of the 10-day precipitation amounts. For the HadRM2 and HadRM3H outputs this was done in different ways. A non-linear transformation of the observed 10-day precipitation amounts was applied to reproduce the changes in the coefficient of variation (CV) occurring in the HadRM2 simulations. The relative increase of the 1000-year annual maximum flow from the resulting scenario was more than twice as large as that from the scenario accounting for the changes in the mean temperature and mean precipitation only. For the HadRM3H model, the bias-corrected model output was used as a scenario. This scenario resulted in a much smaller increase in the 1000-year event than a simple perturbation of the control simulation with the changes in the seasonal mean values.

Mainly because of the large influence of the changes in precipitation variability on the distribution of the annual maximum flows, there were large differences between the estimated changes in the quantiles of this distribution from the two regional climate models. For the HadRM2 experiment, the increase in the 1000–year event was as large as 37% if the increase in the CV of the 10-day precipitation amounts was taken into account. The increase in this quantile was only about 10% for the direct model output of HadRM3H, partly because the effect of the increase in mean winter precipitation was counterbalanced by a decrease in the CV of the 10-day precipitation amounts. It should be noted, however, that it is uncertain

whether a discharge as high as 37% above the present design discharge can pass the Lower Rhine (from Bonn up to Lobith), without causing severe inundations along the river stretch. It is expected that after completion of flood protection works around 2015, a discharge greater than 18,000 m^3/s (or 11% above the present design discharge) will cause flooding along this river stretch (Silva, 2003).

The decrease in the mean summer discharge leads to an increase in the number of days with limitations for inland navigation, in particular for the HadRM3H scenarios for which a decrease in the mean summer flows as large as 40% was obtained. A rough calculation showed that the increase in summer drought in these scenarios results in an increase in the average transport costs of more than 400 Million euro per year. The method of scenario construction has little influence on the magnitude of the impacts from the increased frequency of low flows.

During this study a number of problems were identified that require further attention. Although it was clear that a simple perturbation of the observed data with the change in the seasonal mean values is generally inappropriate when the design discharge is of interest, it is not obvious what the most promising alternative is. The more advanced time series perturbation applied to the HadRM2 data in this study assumes that the 10-day precipitation amounts follow a Weibull distribution. Departures from this assumption may lead to biases regarding the changes in extremes. Though it is in principle possible to achieve any desired change in the shape of the precipitation distribution with a non-linear transformation, this is generally not sufficient if the spatial correlations of the 10-day precipitation fields also change, e.g. due to an increase of the contribution of convective precipitation to the 10-day amounts. An advantage of perturbing the precipitation and temperature data for the present-day climate can be that it leads to a positive correlation between the simulated river flows for the present and future climate. For the distribution of the annual maximum flows at Lobith, this correlation appeared, however, not strong enough to achieve a considerable reduction in the uncertainty of the change in its quantiles. It is expected that this holds more general for river systems where antecedent conditions (soil water and snow storage) have a large influence on peak flows. The direct use of the regional climate model output may be a good alternative to advanced perturbation methods. The distributions of the 10-day precipitation amounts in the present-day climate were reasonably reproduced after a simple bias correction of the HadRM3H control runs. The use of potential evaporation from the Penman-Monteith method led to a bias in the mean summer flows because of a too strong dependence with the soil moisture simulated by RhineFlow. Although this bias could be suppressed by deriving potential evaporation from temperature only, there remained a too strong persistence of dry and wet conditions in the HadRM3H simulations. Hay and Clark (2003) mentioned a similar difficulty with the direct use of regional climate model data.

Because of their large impact on the peak flows, potential changes in the *CV* or, more general, the upper tail of the distribution of the 10-day precipitation amounts need further study. The results from the HadRM2 and HadRM3H experiments and those of Räisänen (2002) for monthly totals suggest that a large part of the changes in *CV* can be attributed to changes in the frequency of dry days. Since the changes in rainfall occurrence are partly linked to changes in the large-scale circulation, it is important to consider different global climate models. For climate change scenario construction the link between the change in *CV* and the change in the mean is of interest. In particular, it would be interesting to know how far a relatively strong increase in the mean will be accompanied by a decrease in *CV*.

The large differences in the changes of the precipitation distributions between climate model simulations are not the only source of uncertainty about the change in the design discharge. Large quantiles of the distribution of the annual maximum flows cannot be accurately determined from a short sequence of simulated river flows. The use of several ensemble members reduces the uncertainty about such quantiles. Resampling techniques offer another possibility to lower the uncertainty of the design discharge. Using a simple stochastic daily rainfall model, Buishand (2003) showed that a considerable reduction in the standard error of a large quantile of the 10-day annual maximum amounts could be achieved by resampling the daily values. A multi-site weather generator for the Rhine basin based on nearest-neighbour resampling has been developed to generate long daily sequences for present-day conditions (Wójcik et al., 2000; Beersma, 2002).

There is a considerable uncertainty about the change in potential evaporation in the future climate. The influence of the change in potential evaporation was, however, relatively small compared to that of the change in precipitation, not only for the design discharge but also for the additional transport costs for inland navigation. For the latter, the potential decrease in summer rainfall is an important, but uncertain factor. The large decrease in summer rainfall in the HadRM3H simulations could, however, be questioned because of a too strong hydrological feedback in the control climate. Apart from the need for more reliable climate model output, it is also desirable to improve the hydrological modelling of low flows.

Acknowledgments

The authors wish to thank H. Buiteveld for his advice and help during the project. The HadRM2 and HadRM3H data were supplied by the Climate Impacts LINK project, DOE Contract EPG 1/11/16 and DEFRA Contract EPG 1/1/124, on behalf of the Hadley Centre and UK Meteorological Office. The meteorological data were made available by the following institutions: Deutscher Wetterdienst, Service de la météorologie et de l'hydrologie de Luxembourg, Météo France and Swiss Meteorological Institute, via the CHR. This research was, in part, supported by the EU Energy, Environment and Sustainable Development programme (contract: EVK1-CT-2000-00075, SWURVE) and the Institute for Inland Water Management and Waste Water Treatment (RIZA), Lelystad.

APPENDIX A
Re-computation of potential evaporation for the HadRM3H simulations

Potential evaporation for the HadRM3H simulations was provided by the Climatic Research Unit. This potential evaporation showed an unrealistic increase in the future climate (section 3.3). It was also not possible to reproduce the mean summer discharge because of a strong correlation between the provided potential evaporation and the simulated soil moisture by RhineFlow (Section 4). Therefore E_p was re-computed using a regression of the reference evaporation E_r on temperature as follows:

1. A regression relationship was estimated for each calendar month and each grid box. Figure A1 shows a scatter plot of E_r and temperature for a grid box in the centre of Germany for the month of August. Altogether 90 points are shown, corresponding to a 30-year period with three 10-day periods in each year. The regression was done on the

anomalies, so with the mean E_r and temperature (over these 90 points) subtracted. The regression coefficient (the slope of the fit) is denoted α_{local}.

2. The regression coefficients were averaged over the Rhine basin, giving α_{area}. This spatial averaging is done to filter out noise.

3. Due to the spatial averaging all spatial information is lost. This leads to problems over mountainous areas where the mean values of E_r are low, causing negative values of the re-computed E_r when the relatively large area-mean α_{area} is used. Therefore, a local correction is applied based on the local 30-year average reference evaporation $\overline{E}_{r,local}$ for the month of interest divided by the 30-year area-average reference evaporation $\overline{E}_{r,area}$ for that month.

4. The evaporation anomaly $\Delta E_r(t)$, with respect to the local mean for the month of interest, is computed from

$$\Delta E_r(t) = \alpha_{area} \frac{\overline{E}_{r,local}}{\overline{E}_{r,area}} \Delta T(t), \quad t = 1,\ldots,36J \tag{A1}$$

with $\Delta T(t)$ the temperature anomaly (again compared to the local mean for the month of interest).

The values from the Thornthwaite formula for the Swiss part of the basin could not be used for the estimation of the spatial average relationship in step 2. They were, however, included in the area-averages $\overline{E}_{r,area}$.

The relative domain-averaged changes in E_r per degree (basin mean change divided by the basin mean E_r) are shown in Figure A2. For the summer, this relative change is about half the relative change that one gets with the application of the Penman-Monteith equation to the HadRM3H output.

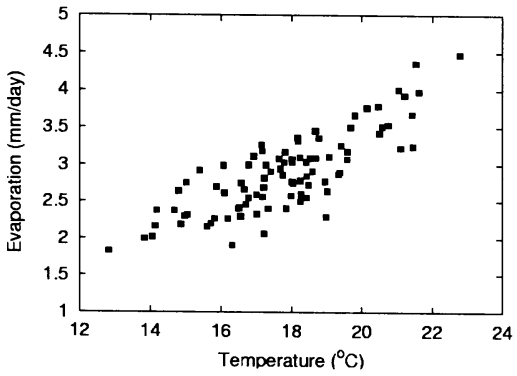

Figure A1. Scatter plot of reference evaporation E_r against temperature for each 10-day period in August for a grid box in the centre of Germany

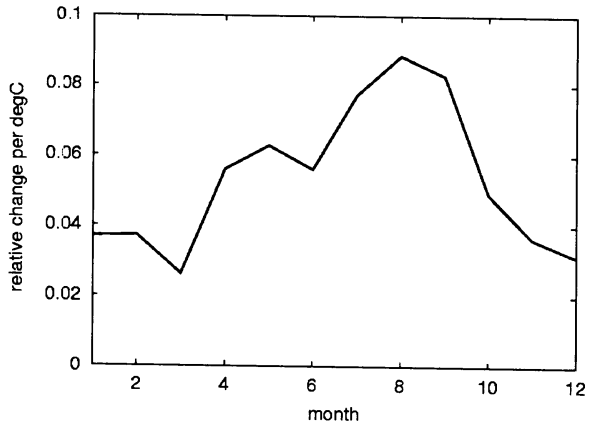

Figure A2. The relative domain-averaged change in E_r per degree (basin-average change divided by basin-average E_r) for each calendar month.

The extrapolation of a regression of evaporation on temperature for the present climate to the future climate is questionable. It may lead to an overestimation of the change in evaporation (Brandsma, 1995). Therefore, apart from the evaporation – temperature regression, two alternative evaporation scenarios were considered. All evaporation scenarios were developed from Eq. (A1) as follows.

The temperature anomalies in the right-hand site of Eq. (A1) can be split into a contribution of the mean temperature change between future and control climate, $\overline{T}_{\text{fut}} - \overline{T}_{\text{cont}}$ (as a function of time of the year and location), and a remaining part accounting for variations in the weather:

$$\Delta T_{\text{fut}}(t) = T_{\text{fut}}(t) - \overline{T}_{\text{cont}} = \left[\overline{T}_{\text{fut}} - \overline{T}_{\text{cont}}\right] + \left[T_{\text{fut}}(t) - \overline{T}_{\text{fut}}\right], \quad t = 1,\ldots,36J \tag{A2}$$

where $T_{\text{fut}}(t)$ are the simulated 10-day temperatures for the future climate. The scenarios for the future E_r were obtained by multiplying the mean temperature change related contribution by a factor β:

- $\beta = 0.0$ (low scenario). This scenario represents a lower limit giving no change in the mean E_r.
- $\beta = 0.5$ (middle scenario), giving an increase of about 25% in E_r in summer, or nearly 4% per °C, which is very similar to the estimate of Brandsma (1995) used in the HadRM2 scenarios.
- $\beta = 1.0$ (high scenario), representing an extrapolation of the present evaporation - temperature relation to the future climate.

Crop factors were then used to convert the E_r values to potential evaporation.

APPENDIX B
The HadRM2 scenario 2 for precipitation

The Weibull distribution is a flexible 2-parameter distribution on the interval [0, ∞). The distribution is given by:

$$F(x) = \Pr(X \le x) = 1 - \exp[-(x/\alpha)^c], \qquad x \ge 0. \tag{B1}$$

Here α is the scale parameter and c the shape parameter. The distribution function can be easily inverted. For the pth quantile x_p we get:

$$x_p = \alpha[-\ln(1-p)]^{1/c}. \tag{B2}$$

For the present climate, the parameters $\alpha = \alpha_0$ and $c = c_0$ were chosen such that the distribution preserves the mean and variance in the observed data, and hence, *CV*. This was done for each 10-day period of the year and for each HadRM2 grid box. For scenario 2, the mean and *CV* were adjusted according to their relative changes in the HadRM2 experiment and then the Weibull parameters α_s and c_s were calculated. It was further assumed that if the observed 10-day amount x_0 corresponds to the pth quantile in the observational series, then the scenario value x_s corresponds to the pth quantile in the scenario series. From Eqs. (B1) and (B2) it follows:

$$x_s = \alpha_s[-\ln(1-p)]^{1/c_s} = \alpha_s[-\ln(e^{-(x_0/\alpha_0)^{c_0}})]^{1/c_s} = \alpha_s[x_0/\alpha_0]^{c_0/c_s}. \tag{B3}$$

If $c_s = c_0$, then HadRM2 scenario 1 (proportional adjustment) is obtained. An increase in *CV* as found in section 3.3 implies that $c_s < c_0$, and thus the exponent in (B3) is greater than 1. This leads to a relatively large adjustment of high 10-day precipitation amounts compared to proportional adjustment. It also leads to an increase in the proportion of very small 10-day precipitation amounts, being somewhat in line with the increase in the number of dry days in the HadRM2 climate change experiment.

The non-linearity of Eq. (B3) hampers its direct application to the RhineFlow grid. The changes in precipitation resulting from aggregating the perturbed values from the RhineFlow grid within a HadRM2 box may differ from those originally projected by HadRM2. To avoid this inconsistency, the ratios x_s / x_0 from (B3) were computed for the observed precipitation amounts aggregated within each HadRM2 grid box and then the scenario series were produced by multiplying the observed precipitation amounts in each grid box of RhineFlow with the ratio x_s / x_0 from the corresponding HadRM2 grid box.

References

Allen RG, Smith M, Pereira LS, Perrier A (1994) An update for the calculation of reference evapotranspiration. ICID Bulletin 43: 35-92

Beersma JJ (2002) Rainfall generator for the Rhine basin: description of 1000-year simulations. KNMI-publication 186-V, KNMI, De Bilt

Beersma JJ, Buishand TA (1999) A simple test for equality of variances in monthly climate data. J Climate 12:1770-1779

Brandsma T (1995) Hydrological impact of climate change, a sensitivity study for the Netherlands. PhD thesis, Delft University of Technology

Buishand TA (2003) Estimation of a large quantile of the distribution of multi-day seasonal maximum rainfall: can stochastic simulation be of use? Memorandum KA-03-02. KNMI, De Bilt (unpublished document)

de Bruin HAR (1987) From Penman to Makkink. In: Hooghart JC (ed) Evaporation and Weather. Proceedings and Information No. 39, TNO Committee on Hydrological Research, The Hague, pp 5-31

Droogtestudie Nederland (2003) Technisch spoor: Eindrapport fase 1, verkenning. Arcadis Ruimte en Milieu, HKV lijn in water en RIZA. RIZA report 110605/ Br 3/ 341/ 000006/ 001, Lelystad

Durman CF, Gregory JM, Hassell DC, Jones RG, Murphy JM (2001) A comparison of extreme European daily precipitation simulated by a global and a regional climate model for present and future climates. Quart J Roy Meteorol Soc 127:1005-1015

Ekström M, Jones PD, Fowler HJ, Lenderink G, Buishand TA, Conway D (2004) Regional climate model data used within the SWURVE project 1: projected changes in seasonal patterns and estimation of PET. *Hydrol. Earth Syst Sci* (submitted)

Frei C, Christensen JH, Déqué M, Jacob D, Jones RG, Vidale PL (2003) Daily precipitation statistics in regional climate models: Evaluation and intercomparison for the European Alps. J Geophys Res 108 (D3), 4124, doi:10.1029/2002JD002287

Gallardo C, Arribas A, Prego JA, Gaertner MA, de Castro M (2001) Multi-year simulations using a regional-climate model over the Iberian Peninsula: Current climate and doubled CO_2 scenario. Quart J Roy Meteorol Soc 127:1659-1681

Giorgi F, Hewitson B, Christensen J, Hulme M, von Storch H, Whetton P, Jones R, Mearns L, Fu C (2001) Regional climate information – evaluation and projections. In: Houghton JT, Ding Y, Griggs DJ, Noguer M, van der Linden PJ, Dai X, Maskell K, Johnson CA (eds.) Climate Change 2001: The Scientific Basis. Contribution of Working Group I to the Third Assessment report of the Intergovernmental Panel on Climate Change, Cambridge University Press, Cambridge, pp 583-638

Grabs W (ed) (1997) Impact of Climate Change on hydrological regimes and water resources management in the Rhine basin. CHR report I-16, Lelystad

Harter HL, Moore AH (1968) Maximum-likelihood estimation, from doubly censored samples, of the parameters of the first asymptotic distribution of extreme values. J American Stat Association 63:889-901

Hay L, Clark MP (2003) Use of statistically and dynamically downscaled atmospheric model output for hydrologic simulations in three mountainous basins in the western United States. J Hydrol 282:56-75

Johns TC, Carnell RE, Crossley JF, Mitchell JFB, Senior CA, Tett SFB, Wood RA (1997) The second Hadley Centre coupled ocean-atmosphere GCM: Model description, spinup and validation. Climate Dyn 13:103-134

Johns TC, Gregory JM, Ingram WJ, Johnson CE, Jones A, Lowe JA, Mitchell JFB, Roberts DL, Sexton DMH, Stevenson DS, Tett, SFB, Woodage MJ (2003) Anthropogenic climate change for 1860 to 2100 simulated with the HadCM3 model under updated emission scenarios. Climate Dyn 20:583-612

Kwadijk J (1993) The impact of climate change on the discharge of the river Rhine. KNAG/Netherlands Geographical Studies publ. 171, Utrecht

Kwadijk J, Middelkoop H (1994) Estimation of impact of climate change on the peak discharge probability of the river Rhine. Climatic Change 27:199-224
Kwadijk J, Rotmans J (1995) The impact of climate change on the river Rhine: a scenario study. Climatic Change 30:397-426
Lenderink G, Buishand TA, van Deursen WPA (2004) Estimates of future discharges of the river Rhine using two climate scenario methodologies: direct versus delta approach. *Hydrol. Earth Syst Sci* (submitted)
Mearns LO, Giorgi F, McDaniel L, Shields C (1995) Analysis of the diurnal range and variability of daily temperature in a nested modeling experiment: Comparison with observations and $2\times CO_2$ results. Climate Dyn 11:193-209
Middelkoop H (1999) Estimating the impact of climate change on peak flows in the river Rhine, RIZA report 99.064, RIZA, Lelystad
Middelkoop H (ed) (2000) The impact of climate change on the river Rhine and the implications for water management in the Netherlands. Summary report of the NRP project 952210, RIZA report 2000.010, RIZA, Lelystad
Nakićenović N, Swart R (eds) (2000) Special report on emissions scenarios. Cambridge University Press, Cambridge
Nash JE, Sutcliffe JV (1970) River flow forecasting through conceptual models 1. A discussion of principles. J Hydrol 10:282-290
Noguer M, Jones R, Murphy J (1998) Sources of systematic errors in the climatology of a regional climate model over Europe. Climate Dyn 14:691-712
Prudhomme C, Reynard N, Crooks S (2002) Downscaling of global climate models for flood frequency analysis: where are we now? Hydrological Processes 16:1137-1150
Räisänen J (2002) CO_2-induced changes in interannual temperature and precipitation variability in 19 CMIP2 experiments. J Climate 15:2395-2411
Räisänen J, Hansson U, Ullerstig A, Döscher R, Graham LP, Jones C, Meier HEM, Samuelsson P, Willén U (2004) European climate in the late twenty-first century: regional simulations with two driving global models and two forcing scenarios. Climate Dyn 22:13-31
Rummukainen M, Räisänen J, Bringfelt B, Ullerstig A, Omstedt A, Willén U, Hansson U, Jones C (2001) A regional climate model for northern Europe: model description and results from the downscaling of two GCM control simulations. Climate Dyn 17:339-359
Shabalova MV, van Deursen WPA, Buishand TA (2003) Assessing future discharge of the river Rhine using regional climate model integrations and a hydrological model. Clim Res 23:233-246
Silva W (2003) Hoeveel (hoog)water kan ons land binnenkomen via de Rijn bij Lobith, nu en in de toekomst. RIZA report 2003.015, RIZA, Lelystad
Thornthwaite CW, Mather JR (1957) Instructions and tables for computing potential evapotranspiration and the water balance. In: Publications in Climatology, Vol. 10, Laboratory of Climatology, Drexel Institute of Technology, Centerton, NJ, pp 183 – 243
UKCIP (2002) Climate change scenarios for the United Kingdom. The UKCIP02 Scientific Report, Tyndall Centre, School of Environmental Sciences, University of East Anglia, Norwich
van Deursen WPA (2003) Klimaatveranderingen in de stroomgebieden van Rijn en Maas: Modelstudies met Rhineflow-3 en Meuseflow-2. Carthago Consultancy, Rotterdam
van Deursen WPA, Kwadijk J (1993) RHINEFLOW: an integrated GIS water balance model for the river Rhine. In: Kovar K, Nachtnebel HP (eds.) Application of Geographic Information Systems in hydrology and water resources management. IAHS publ. 211,

IAHS Press, Institute of Hydrology (now: Centre for Ecology and Hydrology). Wallingford, pp 507-519

Vidale PL, Lüthi D, Frei C, Seneviratne S, Schär C (2003) Predictability and uncertainty in a regional climate model, J Geophys Res, 108 (D18), 4586, doi: 10.1029/2002JD002810

Wójcik R, Beersma JJ, Buishand TA (2000) Rainfall generator for the Rhine basin: multi-site generation of weather variables for the entire drainage area. KNMI-publication 186-IV, KNMI, De Bilt